Ring Imaging Čerenkov Detector Subsystem

RICH Collaboration[1]

Progress Report on Development of Solid Photocathodes and Construction of a Prototype RICH Detector

D.F. Anderson, S. Kwan, and J.G. Morfin

Fermi National Accelerator Laboratory, Batavia, IL 60510

B. Hoeneisen

Universidad San Francisco de Quito
P.O. Box 841, Suc. 12 Octubre, Quito, Ecuador

G. Alley, H. Brashear, and C. Britton

Oak Ridge National Laboratory, Oak Ridge, TN 37831

N. S. Lockyer, J. Millan, and S. Peil

Department of Physics, David Rittenhouse Laboratories, University of Pennsylvania, Philadelphia, PA, 10104

W.S. Anderson, E. Dunn, J.G. Heinrich, C. Lu, K.T. McDonald, and Y. Zhu

Joseph Henry Laboratories, Princeton University, Princeton, NJ 08544

A. Lopez, C. Hernandez, A. Mendez, and J. Palathingal

Department of Physics

and

R. Palomera-Garcia

Department of Electrical Engineering
University of Puerto Rico, Mayaguez, Puerto Rico, 00708

[1]Contact Persons: J. G. Morfin and N. S. Lockyer

Executive Summary

Hadron identification is a critical component of any B detector at the SSC designed to study CP violation. Kaon identification is particularly efficient for tagging the particle-antiparticle nature of the other B in CP-violation studies. High-rate Ring Imaging Čerenkov detectors (RICH) provide the solution. We have been pursuing a breakthrough in solid-photocathode technology developed by us; low-pressure operation of a solid, roughly 1-μm-thick, Cesium Iodide (CsI) photocathode plus a monolayer of adsorbed TMAE. This photocathode has extremely fast time response and can be coupled to a relatively simple parallel-plate chamber with instrumented cathode pads for readout. In the past year we have:

- Studied the basic properties of thin CsI + TMAE photocathodes, including the aging rate, quantum efficiency, and time response.
- Designed, constructed, and begun testing the first full-prototype RICH detector using a solid photocathode inside a low-pressure parallel-plate chamber with VLSI readout.
- Begun the study of novel photocathodes, such as 'sponge' photocathodes.

In FY92 we propose to continue and extend these studies and seek \$110k for Fermilab, \$50k for Oak Ridge, \$121k for Pennsylvania, \$106k for Princeton, and \$53k for Puerto Rico, totalling **\$440k** for R&D with the following goals:

- Construct a new prototype with improved engineering: better vacuum design, improved vacuum feedthroughs, use of low-Z materials, and large-area thin-window construction (Penn).
- Construct and test-resistive cathode pads for the RICH in 1-D and 2-D (Penn and Puerto Rico).
- Continue studies of the cathode properties: aging, timing and quantum efficiency (Fermilab).
- Build a combined time-of-flight and RICH prototype (Fermilab).
- Fabricate a prototype VLSI readout chip set for the RICH pad plane (Oak Ridge and Puerto Rico).
- Explore the utility of 'spongelike' materials for photocathodes and the use of solid-TMAE photocathodes in liquid xenon (Princeton).

Contents

List of Figures

1 Introduction

The interest in pursuing B physics in a hadron collider continues to increase as CDF demonstrates its ability to observe exclusive decay channels. Presently, two decay modes have been demonstrated, and more are expected in the next run. This success improves the likelihood of a dedicated B collider detector at the SSC. However, in order to achieve sensitivity over the full range, 10%-30%, of CP asymmetries expected in the standard model from $B \to J/\psi K^0_S$, tagging of the 'other' B via the sign of the $K^{\pm}$ decay product has been shown to be necessary. The RICH counter provides π and K identification over a greater momentum range than any other technique [1, 2].

The work of D. Anderson, B. Hoeneisen, and S. Kwan at Fermilab and J. Seguinot *et al.* at Cern indicates great promise for the solid photocathode technique [3, 4, 5, 6, 7, 8, 9]. The timing properties of the solid photocathode make it appropriate for the high rates expected at the SSC.

2 Progress Report - Pennsylvania

2.1 Overview

The primary goal of this proposal for FY91 was to perform a system test of a Ring Imaging Čerenkov detector (RICH) based on new developments in the field of solid photocathodes, and to observe a Čerenkov ring from minimum-ionizing particles.

We designed, constructed, and are testing the first full-prototype RICH detector using a solid photocathode inside a low-pressure parallel-plate chamber. The three basic RICH counter components in our design are a pressure vessel, a parallel-plate chamber, and the VLSI-based readout system. Over the last year, we have built several prototype versions of each of the components. These detectors were used primarily as learning devices. The major issue for the pressure vessel was vacuum leaks. We have attempted to bring several hundred readout channels from within the vacuum vessel out to atmospheric pressure in a way that is inexpensive, mechanically stable, and without leaks. The parallel-plate chamber design was quite simple, straightforward and reliable. Finally, the readout system, composed of SVX readout chips, works well, though is sensitive to grounding procedures. It is difficult to shield the vacuum system effectively from RF-noise.

At the present time we have:

- Constructed and tested a prototype low-pressure parallel-plate chamber that operated with gaseous TMAE as the UV absorber.
- Fabricated a steel-mesh parallel-plate chamber inside a pressure vessel suitable for a beam test with the solid photocathode.

- Evaporated CsI and TMAE onto a printed-circuit board containing 332 pad channels (performed at Princeton).
- Fabricated interface boards to feed signal lines out of the vacuum vessel.
- Fabricated printed-circuit boards on which the 8 SVX chips are mounted.
- Measured pedestals on all channels from the 8 SVX chips connected to the chamber. Typical noise levels obtained are $\sim$ 2000 electrons equivalent-noise-charge.
- Observed single-photon signals in the chamber from UV generated by a hydrogen discharge lamp and successfully read them out with all SVX chips connected.

We anticipate a beam test within a few weeks.

2.2 Design Issues

We have begun to study aspects of the RICH design not directly associated with the photocathode aging. There are at least three main issues that require study:

1. The RICH detector must be run at low pressure with a minimum of material used for the pressure vessel.
2. The parallel-plate-chamber design must have high uniform gain over a large physical area.
3. The readout system must accommodate a very large number of channels, and be sensitive to single photoelectrons while minimizing the cost per channel [10].

2.3 Overview of the RICH Prototype

The RICH prototype has been designed to operate at low pressure with a solid photocathode sensitive to ultraviolet wavelengths in the range 180-230 nm. It is composed of three main pieces: the pressure vessel, the parallel-plate chamber, and the readout system, as shown in Fig. 1. The pressure vessel includes a quartz window, a drift space, a steel-mesh anode, the cathode pad plane, and a gas volume for signal amplification. The radiator, liquid C_6F_{14}, is contained in a quartz vial separate from the pressure vessel. The RICH detector operates with proximity focusing (*i.e.*, no focusing) with an optical drift distance of 4 cm. The front-end electronics are 8 LBL SVX chips and the data acquisition is CAMAC based.

During operation the chamber a UV Čerenkov photon traverses the quartz window, the anode-wire mesh, and strikes the cathode pad plane with the solid photocathode on its surface. A single photoelectron is released and drifts in a homogeneous

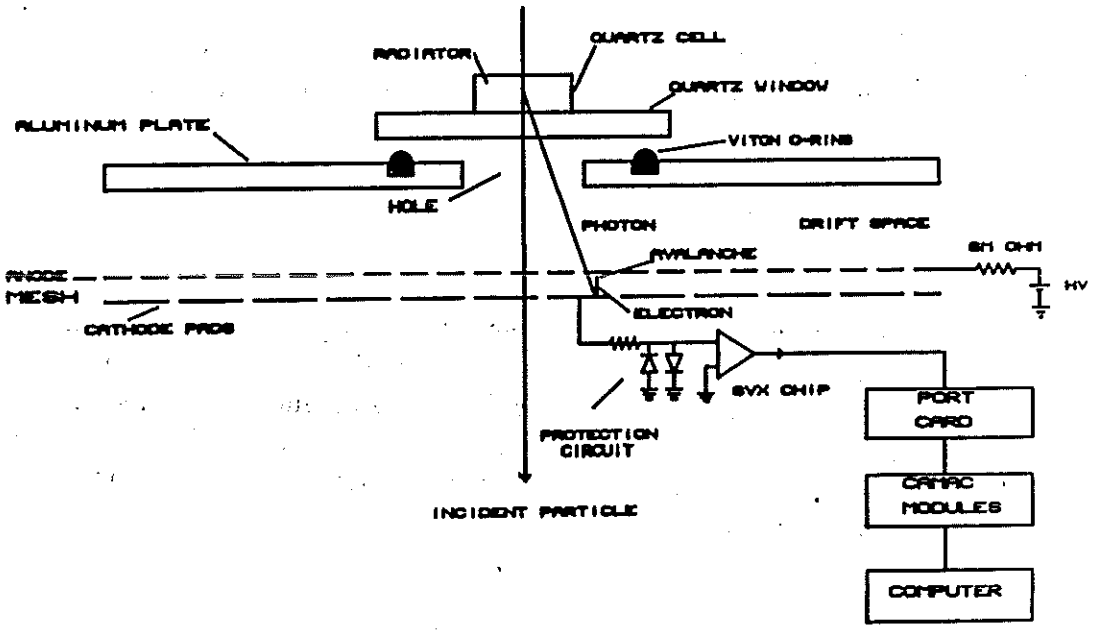

Figure 1: Prototype RICH chamber.

electric field, 2 mm in length, towards the anode mesh which is connected to a positive high voltage. The pad plane has a reference to ground potential through the preamplifier. The low-pressure parallel-plate chamber develops gains from 10^4 to 10^7 depending on the gas and the electric field. The induced positive current on the pad plane is detected and amplified using the SVX charge-preamplifier chip.

The Čerenkov ring seen at the end of the radiator, for photons being emitted at the beginning of the radiator, has a radius

$$r = L_1 \tan\theta_C,$$

where L_1 is the radiator length, and θ_C is the Čerenkov angle. The photons traverse different media before arriving at the pad plane. Applying Snell's law at the boundaries to find the final ring size in the pad plane, we find

$$R = L_{rad} \tan 38° + L_{container} \tan 32.8° + L_{window} \tan 30.7° + L \tan 51.4° = 6.4 \text{ cm},$$

where L is the optical drift distance in vacuum, as shown in Fig. 2.

The resolution on the measurement of the ring radius depends on the pad size, smaller pads giving better resolution. The maximum possible number of channels connected to the SVX chip using our PC-board technology is only 42 out of 128 (see Sec. 3.5.2). Then for 8 SVX chips, and a pad-plane radius of 11.4 cm we instrumented 332 pads of size 9×9 mm^2 with a 1-mm gap between them. Hence the rms spatial resolution will be 2.9 mm.

2.4 Experimental Apparatus

2.4.1 Radiator

For our detector we have chosen C_6F_{14} as a radiator. The index of refraction at 6.5 eV is $n = 1.278$ and γ_{th} is 1.5. The chromatic aberration in the radiator induces a rms smearing of 3 mm on the Čerenkov ring. The number of UV Čerenkov photons is about 25 for a 1-cm-length radiator.

The radiator is contained in a cylindrical spectrophotometer quartz cell from Hellma Cells (Jamaica, NY). The light path is 1.0 cm, the inner diameter of the cell is 1.9 cm, the walls are 0.1-cm thick and the volume is 2.8 ml.

2.4.2 Window

The optical aperture in the aluminum-pressure-vessel is 3.3 cm in diameter. We use a 5.08-cm-diameter, 0.95-cm-thick UV fused-silica (SiO_2) window in the detector. The index of refraction at 220 nm is 1.53. The window was obtained from Janos Technology (Townshend, VT).

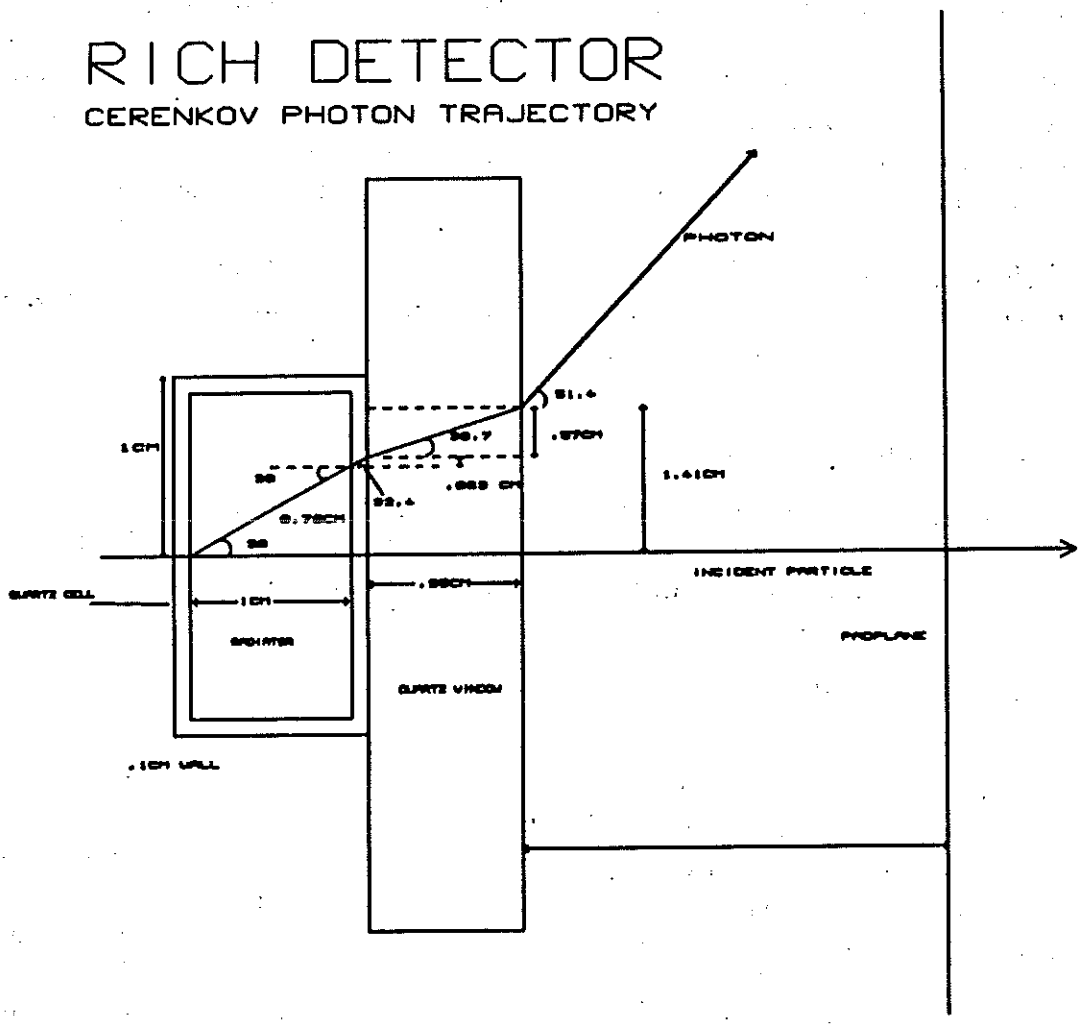

Figure 2: Čerenkov light path from the beginning of the radiator to the pad plane, using Snell's Law.

2.4.3 Solid Photocathode

The solid photocathode is fabricated as follows: The pad plane is cleaned with an abrasive material and ethyl alcohol, mounted in a bell-jar and pumped to a pressure in the order of 10^{-7} torr. A 0.5-μm-thick layer of CsI (as determined by a Sycon STM-100 quartz thickness monitor) was vacuum evaporated onto the cathode pad plane at rate of about 50 Å/sec. Immediately after the evaporation and without breaking the vacuum, the evaporation chamber was filled with TMAE gas to its equilibrium vapor pressure of about 300 mtorr to adsorb a layer of TMAE on the CsI film. The photocathode board was removed from the bell-jar and placed in the detector as rapidly as possible to minimize water absorption. The CsI is 99.999% pure (Aldrich Chemical Co., Milwaukee, WI). Purified TMAE was obtained from D. Anderson at Fermilab, and we used the evaporator of K.T. McDonald at Princeton University.

2.4.4 Anode-Wire Mesh

The anode mesh is a stainless-steel cloth made of 3041 wire, 50 μm in diameter and 80% transparency (Metalweave Inc, Peabody, MA). The mesh was glued onto a G-10 ring, 0.5″ thick, 8″ inner diameter and 9.75″ outer diameter, with DP-190 Epoxy.

2.4.5 Pad Plane

The pad plane is a 11.4-cm-radius, 6-mm-thick circular, two-layer G-10 PC-board. This board is constructed in four quadrants. Layer 1 of the PC-board has the cathode pads, contained in a circle of of 10-cm radius. Each quadrant has 83 copper pads for a total of 332 pads on the pad plane. Plated-through vias carry the signals from Layer 1 to Layer 2, which carries signals to a surface-mount connector. Every trace from the pad to the connector is shielded with ground lines which run on each side of the trace. A solder mask on the traces was deposited to inhibit contact with ground. The PC-board layouts are shown in Figs. 3-4, and were produced using ALS VIEW interactive software. The Gerber files containing the design were sent to Action Circuits (Danbury, CT). The surface mount connectors were obtained from SAMTEC (New Albany, IN).

2.4.6 Vacuum-Vessel Endplate

The vacuum system is shown in Fig. 5.

The stainless-steel cylindrical chamber has three access ports that accommodate the vacuum line, the high voltage feedthrough, and gas input. In addition, there is a 10″-diameter port in the endplate which is used to mount the pad plane, as shown in Fig. 6. This port has four 6-cm-long 1.3-cm-wide oval slots with O-ring groves, that allow access to the connectors mounted to Layer 2 of the pad plane. The seal is made by four Interface Boards (Figs. 7-8) that sealed to the endplate with O-rings.

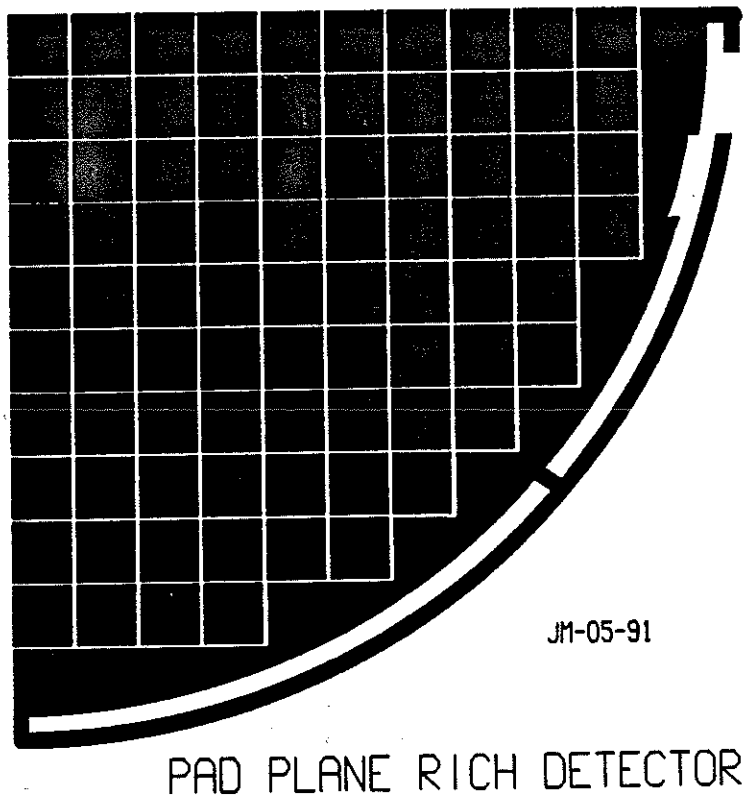

Figure 3: Pad-Plane Layer 1.

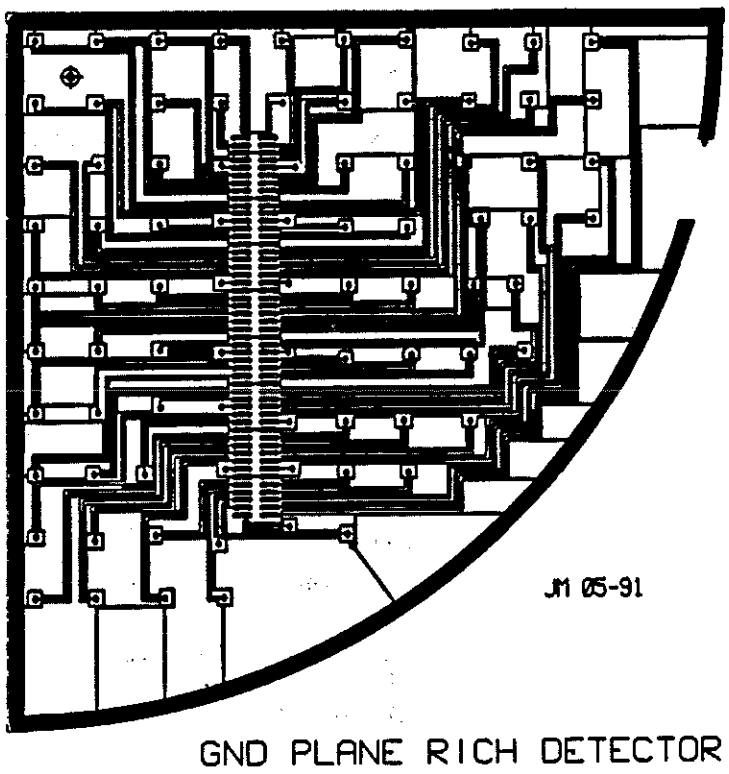

Figure 4: Pad-Plane Layer 2.

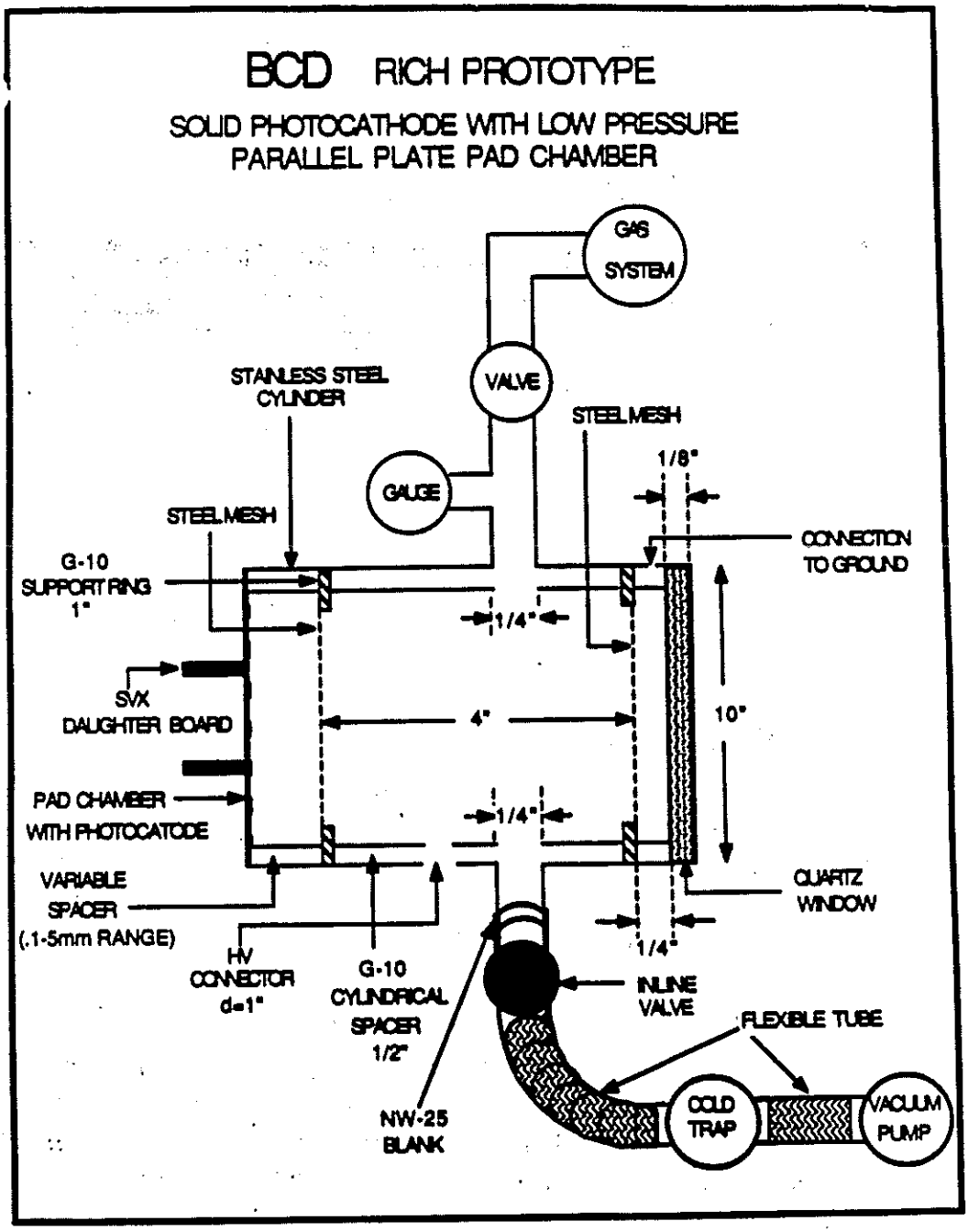

Figure 5: Vacuum-chamber design.

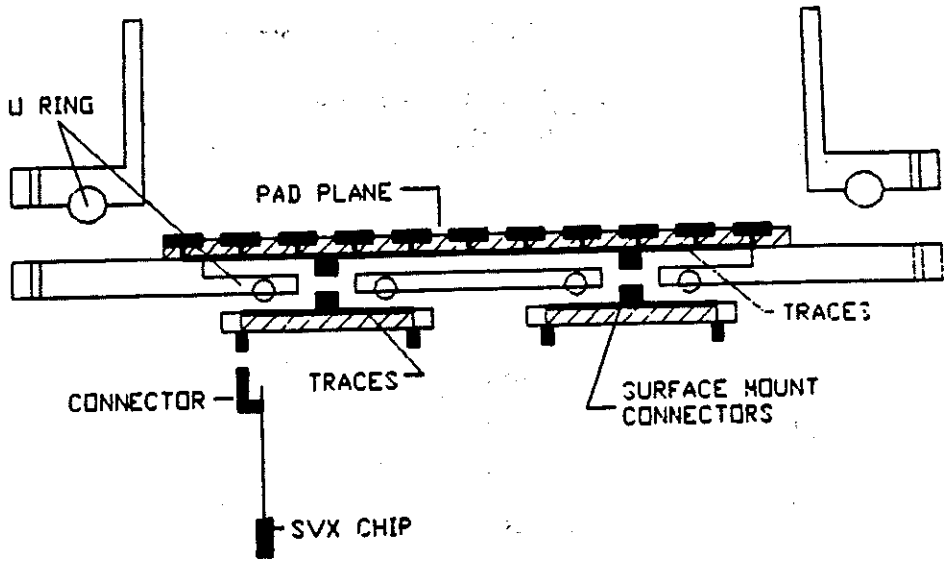

Figure 6: Endplate configuration.

2.5 Readout System

The 332-channel readout system is based on the SVX data-acquisition chip [11] and associated CAMAC modules [12]. To connect the SVX input channels to the pads in the chamber and connect the SVX I/O pads to the data-acquisition system, three interface PC-boards were designed. This section discusses SVX chip characteristics, and the design and layout of the PC-boards.

2.5.1 Front-End Electronics: SVX Data-Acquisition Chip

The SVX chip is a high-density, low-power data-acquisition chip designed to read out data from detectors with input capacitances of up to 30 pf. Each channel is a low-noise, DC-coupled charge integrator with a gain of 14 mV/fC. The chip contains 128 channels on a 50-μm readout pitch. The SVX chip has sparse data scan and a multiplexed serial readout. Up to 64 chips may be chained together.

The chip was operated in double-correlated-sample mode, with an "Integration Window" of 6 μs.

2.5.2 PC-Board Design and Layout

Two PC-boards were designed in order to connect the 8 SVX chips to the pads in the chamber and to interface the chips to the data-acquisition system. Each SVX

chip was mounted on its own Carrier Board and two Carrier Boards are mounted to an Interface Board. The four Interface Boards are mounted one per quadrant on the chamber endplate.

Interface Board

The Interface Board was designed to connect the SVX chip, located outside of the chamber, to the pads inside the chamber. The board is 3-mm thick and consists of two PC-board layers as shown in Figs. 7-8.

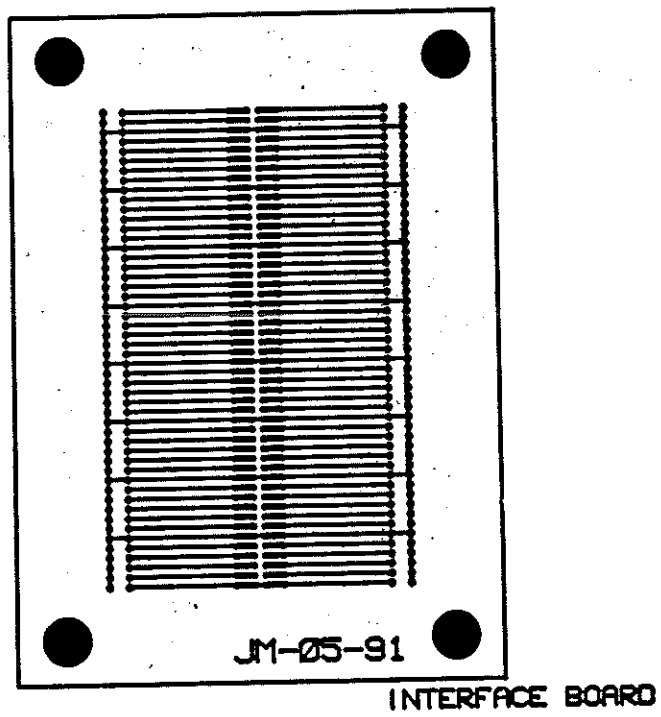

Figure 7: Interface Board Layer 1.

To readout the signal lines we mate the male surface-mount connector on Layer 2 of the cathode-pad-plane PC-board (Fig. 4) to a female surface-mount connector on Layer 1 of the Interface Board.

After the connectors have been mounted on the board, a plastic cover with a slot in the center is glued onto Layer 1. This allows us to have a smooth surface for the O-ring seal. It was found that 5-minute epoxy was slightly conductive and destroyed the SVX pedestals. It was necessary to remove the epoxy and apply Glyptol insulation paint on Layer 1. A solder mask (not shown), was designed to insulate the signal lines from the end plate when the board is connected. In future versions, a smoother mask will be designed to provide a better vacuum seal.

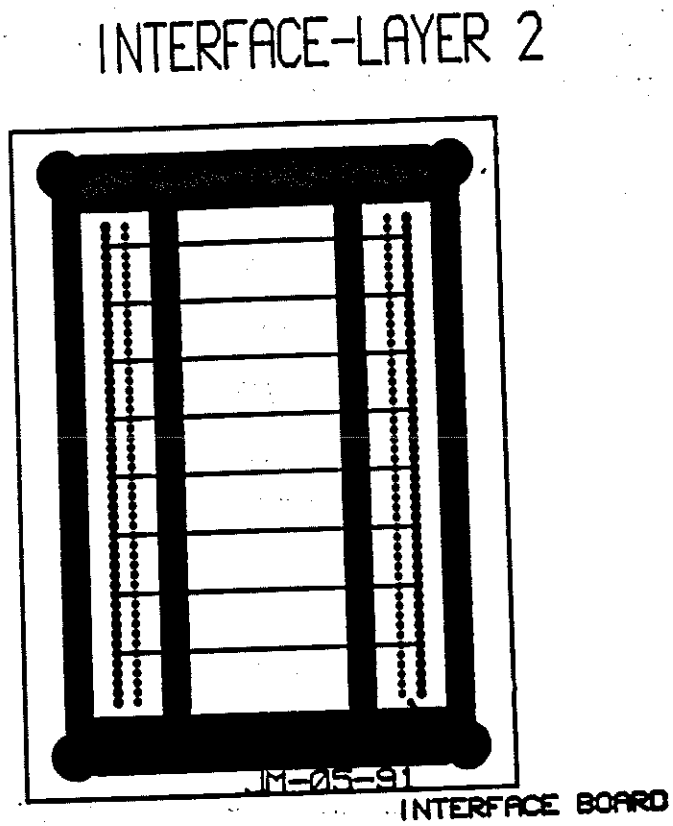

Figure 8: Interface Board Layer 2.

SVX Carrier Board

As mentioned above, the SVX chip has 128 pads for input signals and 31 I/O pads for the control and analog out signals. These pads are on a 0.1-mm pitch. An easily obtained pitch in our PC-board technology is 0.25 mm which permitted only 42 of the 128 channels of the SVX chip to be used. The SVX Carrier Board is shown in Fig. 9.

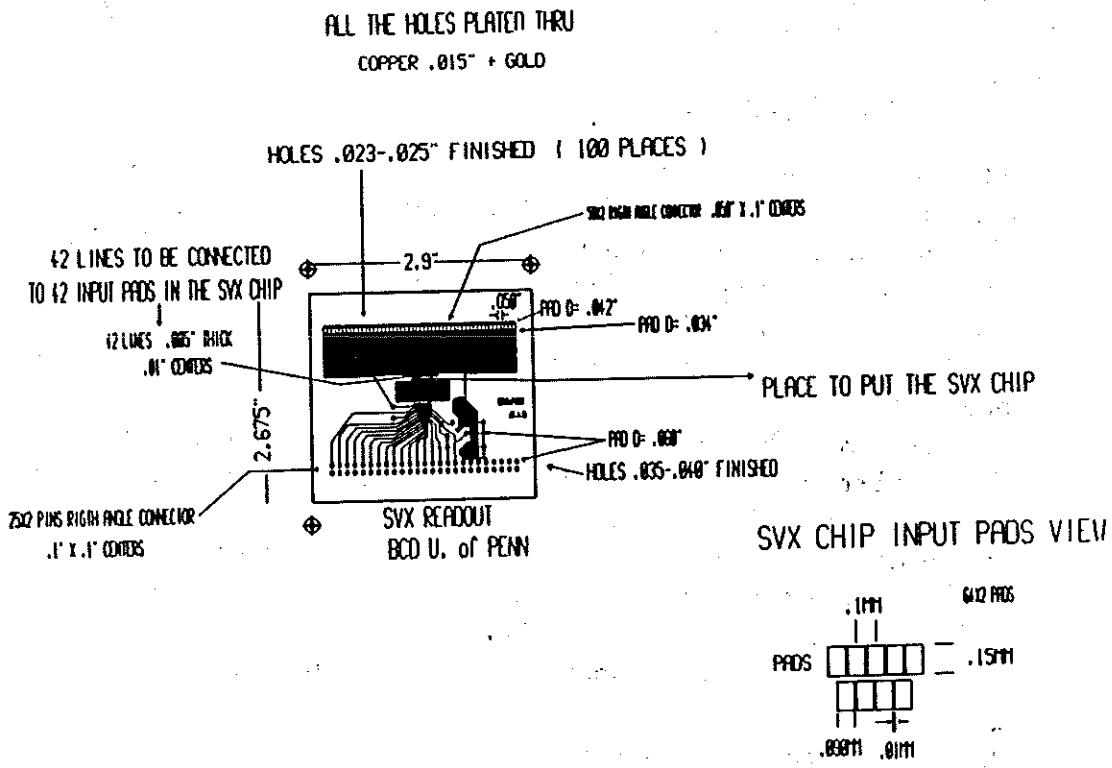

Figure 9: SVX Carrier Board.

The SVX chips were bonded to the Carrier Board by Promex (Santa Clara, CA). The resulting aluminum bonds looked and performed well. The 42 traces are fanned to a right-angle surface-mount connector which mates to either of the two surface-mount connectors on Layer 2 of the Interface Board.

The SVX I/O lines are bonded to pads on the Carrier Board with traces that fan out to a 50-pin flat-cable connector that connects to the data-acquisition system.

2.5.3 Data-Acquisition System

The data-acquisition system is based in the SRS and SDA CAMAC modules designed at LBL [12] and built by the University of Oklahoma for us. The SRS module is used

to produce programmable patterns of control signals for controlling the operation of a group of one or more SVX chips. The SDA module receives, digitizes, and stores analog and digital data signals from the SVX during the readout phase.

2.6 Prototype Chamber Results

We present results on chamber operation, SVX chip performance, and signals from UV photons observed both with an oscilloscope as well as readout through the SVX data-acquisition system.

2.6.1 Configuration

The present operating configuration of the prototype chamber consists of a photocathode made August 16, 1991 at Princeton University, and 7 SVX readout chips. The photocathode is 0.76-μm-thick CsI with a monolayer of TMAE adsorbed on the surface. The prototype-chamber leak rate is very low, about 0.03 torr/hour. We run with pure ethane at 26.5 torr. We evacuate the chamber and refill with ethane about once per week. We have not opened the chamber to atmosphere since making the photocathode.

The SVX is DC-coupled to the pad plane; there is no protection circuit between the chamber pad and the SVX chip. We are presently repairing SVX chip number 8. The chamber gap is 2 mm and we operate at about 580 Volts positive high voltage on the steel mesh. The pad plane is held at ground potential.

The chamber is positioned horizontally with the quartz window facing down. The SVX chips are on top of the chamber in this configuration. All cables are shielded with aluminum foil and we operate with a single ground.

2.6.2 Chamber Operation

The chamber operation has been reliable. The biggest problems were associated with vacuum leaks which have been fixed.

We desire to operate the chamber to see single photons with the SVX chip. We found that a pressure of 26.5 torr ethane and a voltage of 580 V was suitable. Fig. 10 shows the relative gain *vs.* pressure at 26.5 torr, and that the chamber breakdown voltage is about 630 V. As the SVX chips have no breakdown protection, we operate the chamber 50 V below the breakdown voltage.

Testing of the chamber has been done with a hydrogen discharge lamp as a source of UV photons, rather than Čerenkov light. The hydrogen lamp (Hamamatsu, Bridgewater, NJ) delivers a fast (< 3 ns) pulse of about 10^5 photons with wavelengths from 170-400 nm through a quartz window. The hydrogen lamp produces signals on RICH prototype large enough to be seen directly with an oscilloscope (see Fig. 11). The UV lamp operates at a rate of about a 1 kHz, and a trigger pulse was formed by picking up the noise created during the lamp discharge. The hydrogen lamp was located $\sim$5 cm from the quartz window of the RICH chamber.

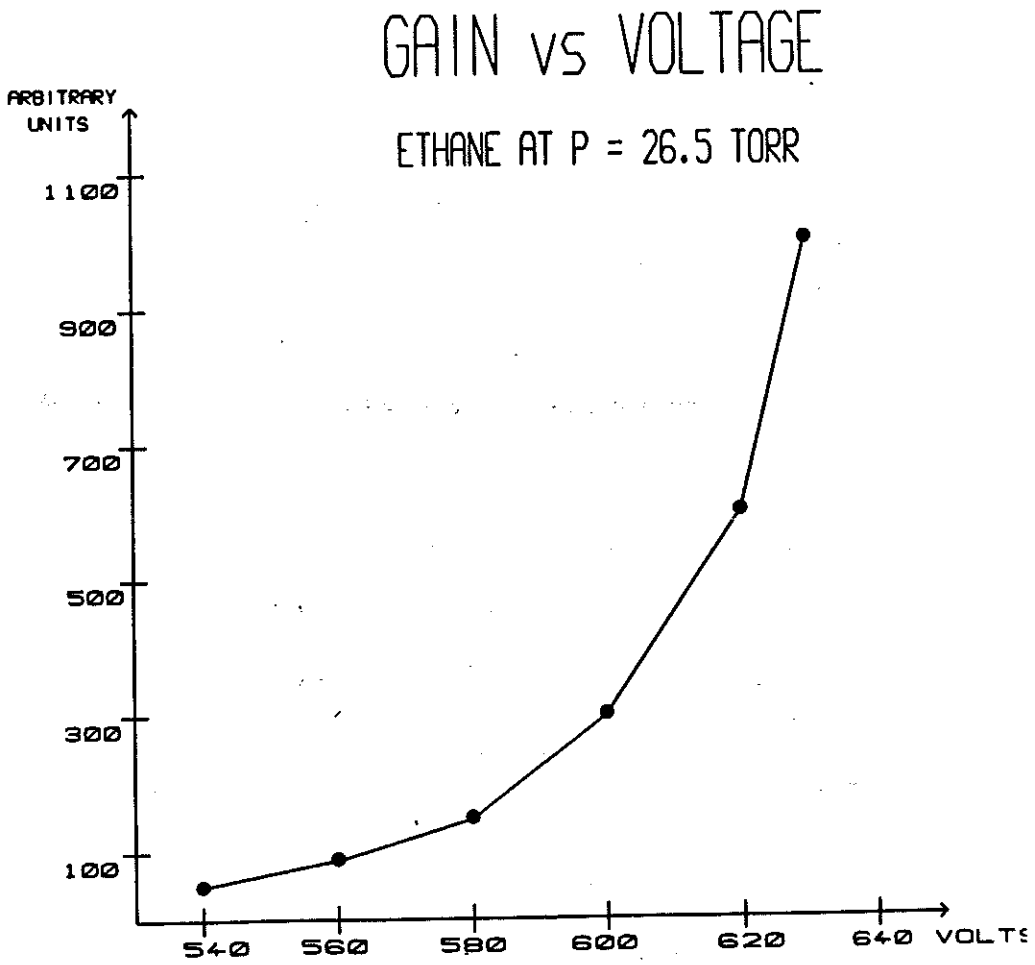

Figure 10: Relative photocathode gain *vs.* voltage.

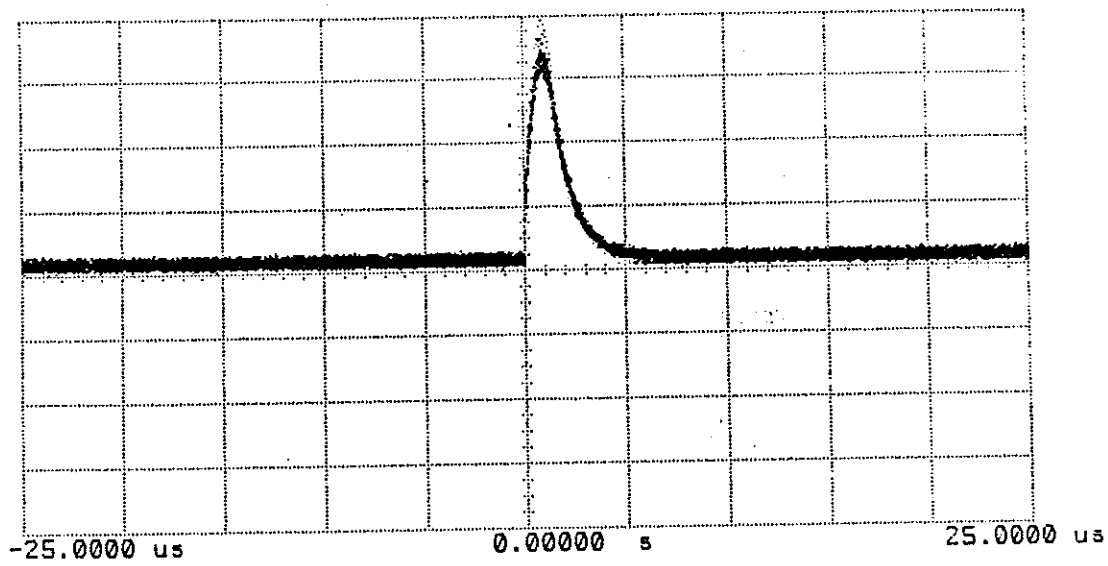

Figure 11: Signal on the photocathode from the hydrogen lamp as observed with an oscilloscope.

2.6.3 SVX Chip Pedestals

Measurement of the SVX chip gain was performed by injecting charge into the 60-ff SVX-calibration capacitor. The charge was injected through an external 15-pf capacitor by applying a positive step voltage. We deduced a gain of 14.9 mV/fC, in agreement with SVX chip specifications.

A scope trace of the SVX analog output in the case of no input is presented in Fig. 12 showing 128 channels of pedestals. Below this signal is the SRS clock signal and scope trigger generated by the microcode. A pedestal-distribution measurement for each SVX chip has been performed using the full data-acquisition program. The measured noise level of a single channel with zero input capacitance is typically 500 electrons, equivalent noise charge, and is shown in Fig. 13. The distribution of pedestals for 4 SVX chips is shown in Fig. 14 and indicates channel-to-channel fluctuations of about 1000 electrons rms.

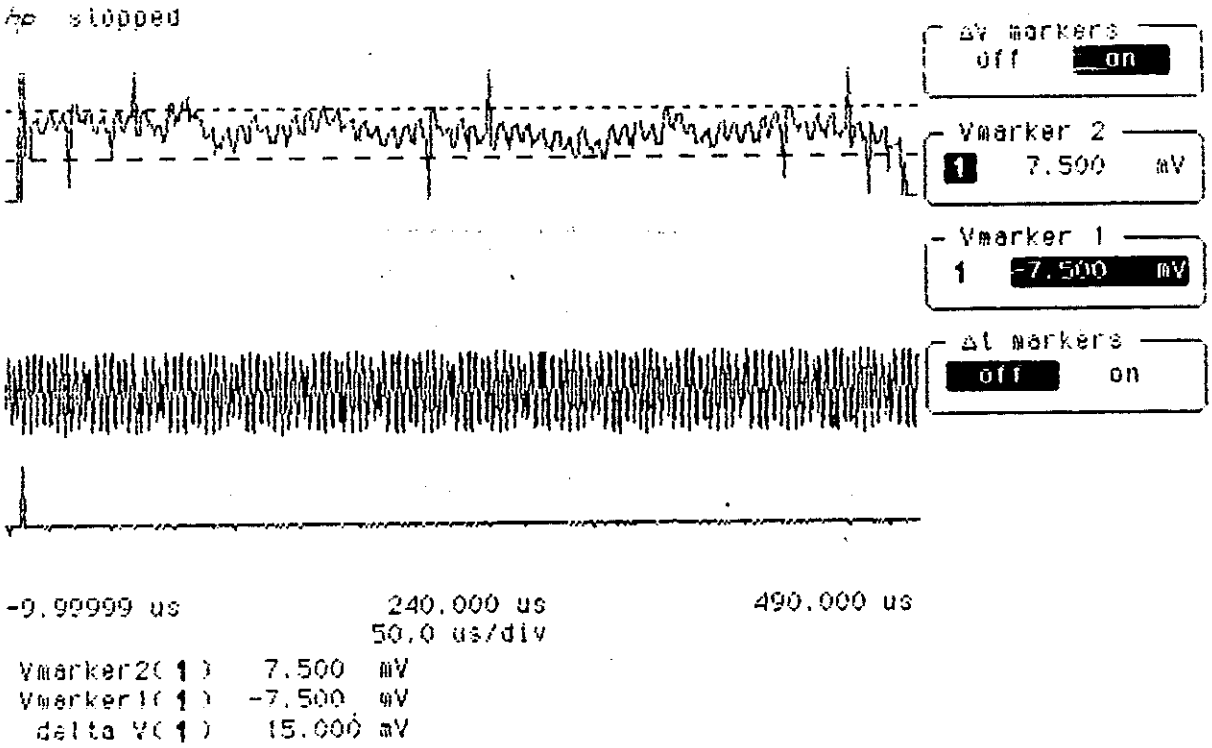

Figure 12: Pedestal distribution for an SVX chip as observed on a digital oscilloscope.

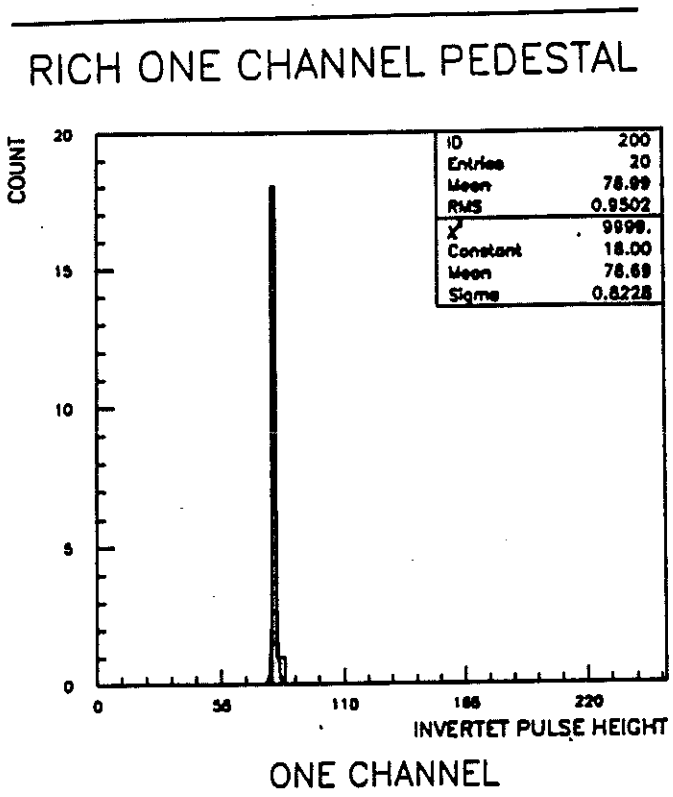

Figure 13: Pedestal distribution for 1 channel. The noise σ of 0.82 counts corresponds to 450 electrons.

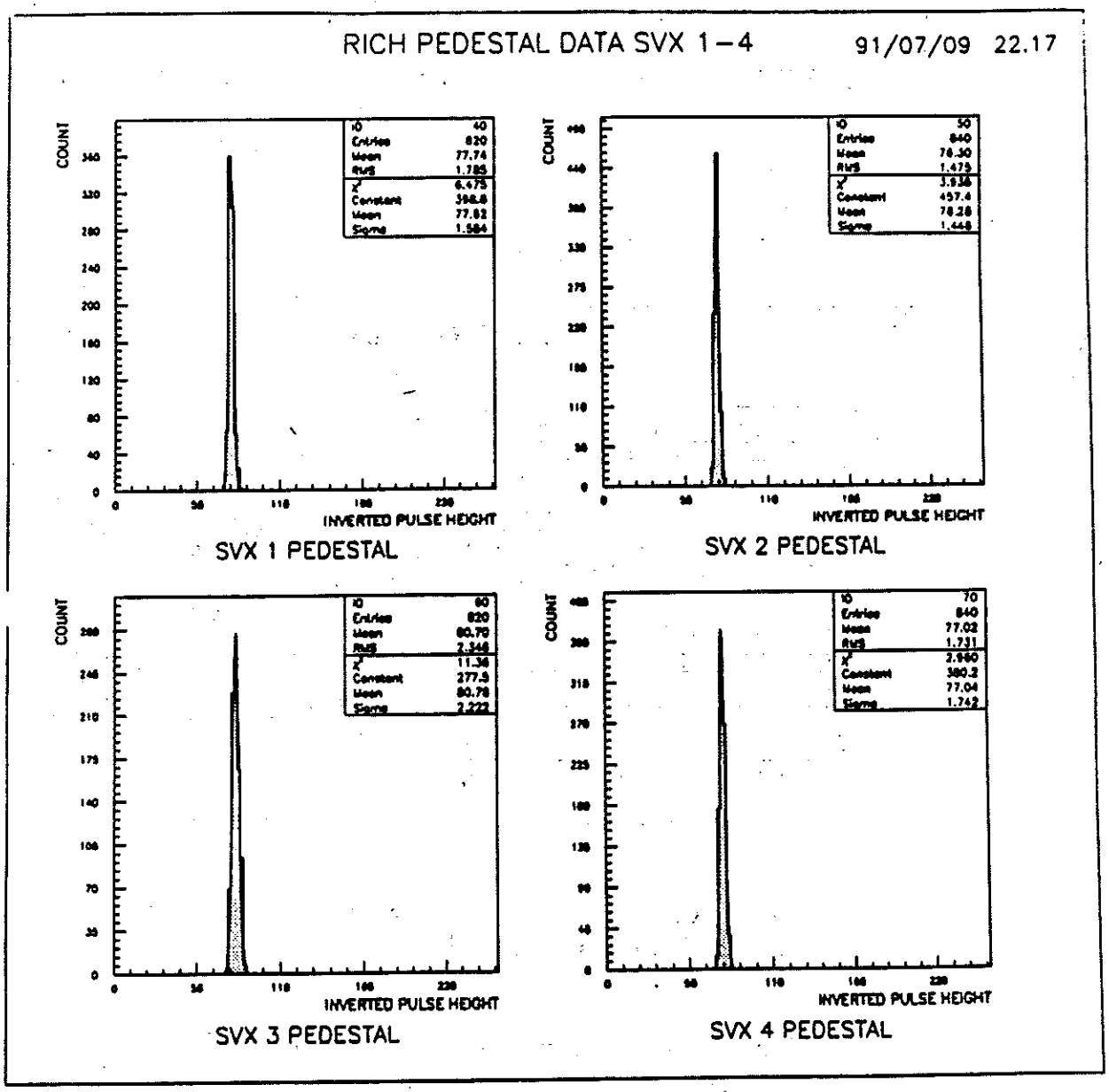

Figure 14: Pedestal distribution averaged over 42 channels for the SVX chips 1-4. The average noise $\sigma = 1.6$ counts.

2.6.4 Detection of UV Photons

We have observed signals from the hydrogen lamp with the full readout chain connected.

The SVX integration window is about 6 μs and the complete readout cycle is about 40 ms, resulting in a duty factor of about 10^{-4}. This will be adequate for the upcoming beam tests, and permits the observation of a single-photon from the UV lamp every 2 minutes.

Figure 15 shows the signal from a multiphoton event from the hydrogen lamp for operation of the RICH chamber with 7 SVX chips.

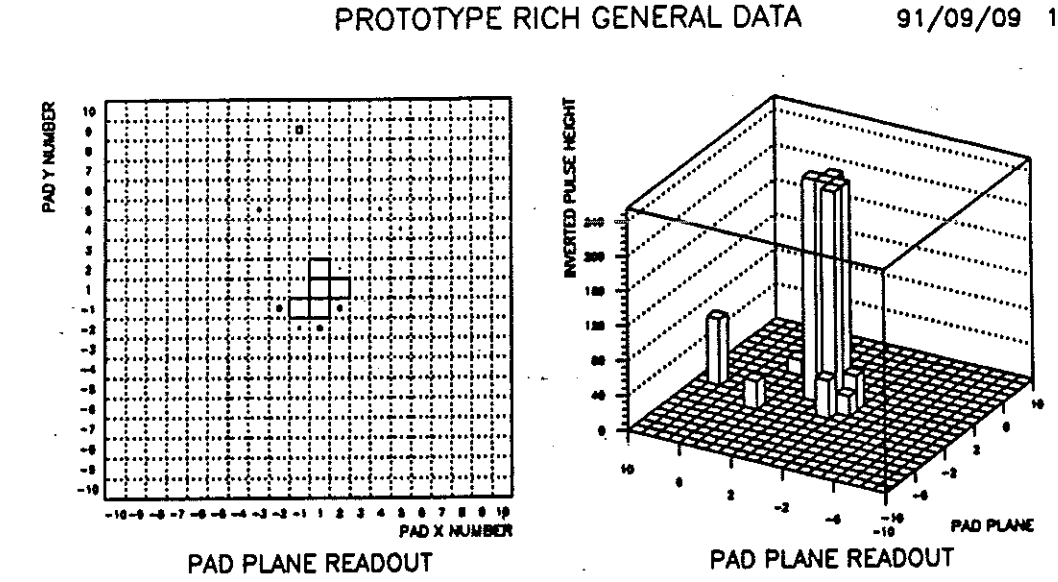

Figure 15: A multiphoton event observed in the prototype RICH chamber with 7 SVX chips connected.

We will study the chamber in the M-Test beam at Fermilab in the next few weeks. We will determine the number of found photoelectrons per minimum-ionizing particle, and see whether the minimum-ionizing track is directly detected by the CsI-TMAE cathode.

2.7 Proposed Research

2.7.1 Continuation of Studies with the First RICH Prototype

We envision several improvements to the design:

1. Replace the present cathode pad plane with smart pads.

2. Redesign the chamber to include a full-area quartz window.

3. Redesign the vacuum feedthrough of the signals from the cathode pads.

4. Incorporate composite materials in chamber design in place of stainless steel.

5. Redesign the SVX Carrier Board to use the Oak Ridge–Puerto Rico readout (see Secs. 6 and 7).

The proposed improvements to the chamber are shown in Figure 16.

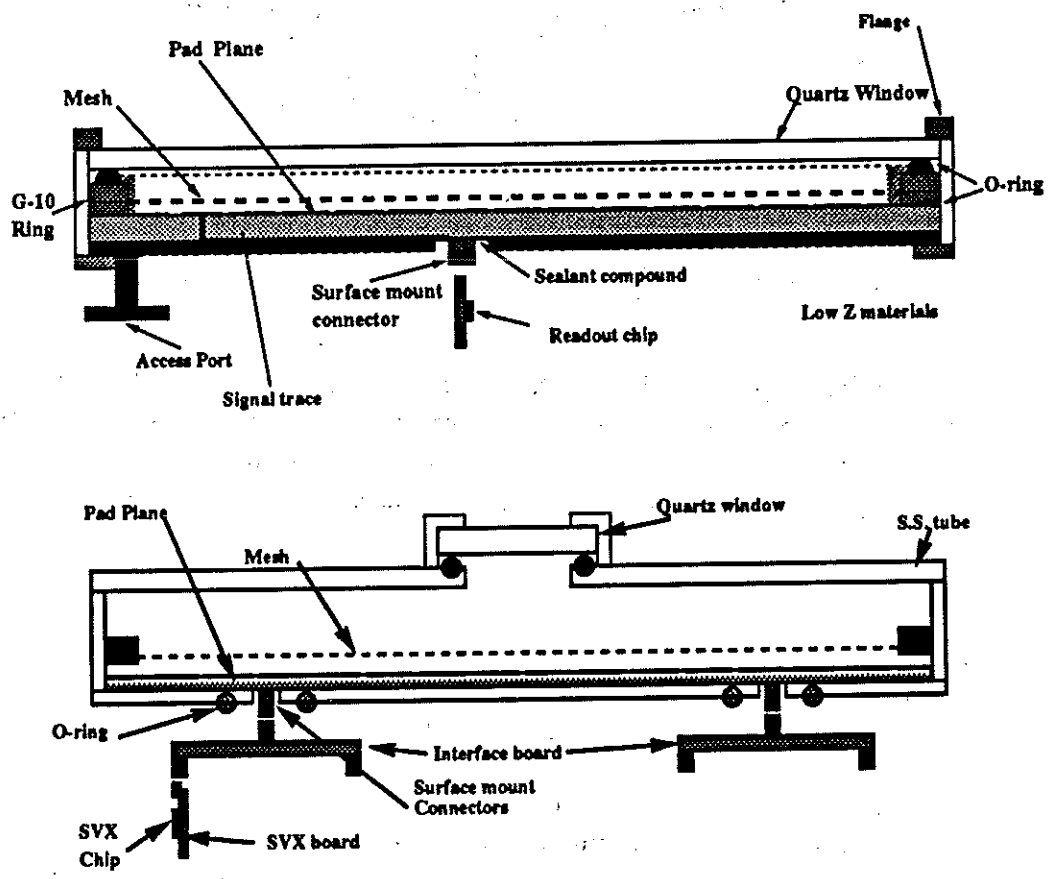

Figure 16: New (top) and old (bottom) designs for the prototype chamber.

The major difference between the old and new designs is the vacuum feedthrough of the pad-plane signals. In the old design, the pad-plane surface-mount connector mated with the Interface Board surface-mount connector. The vacuum seal was made with an O-ring underneath the Interface Board. This was a continual problem because of vacuum leaks. In addition, the connector leaked and the SVX chip was very sensitive to the type of sealant used to seal the connector. **In the new design there is no interface board.** The cathode pad plane is effectively glued to the endplate, and the signals emerge from the vacuum at one slot in the endplate where

the traces are sealed with epoxy. The fabrication of the cathode-plane PC-board must have a flat, laminated surface.

Another difference is the quartz window area and thickness. We attempt in the new design to maximize the acceptance of particle trajectories. We have calculated the window stresses and deflections based on a flat plate supported at the edges. The stress calculation model for the chamber window is shown in Figure 17.

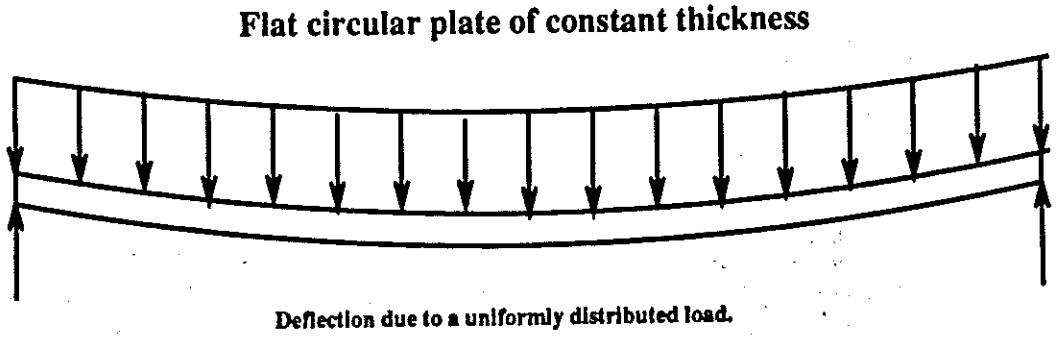

Figure 17: Model for the stress calculation of an edge-supported flat plate.

Finally, we plan to change the chamber geometry from cylindrical to rectangular and to use composite materials rather than stainless steel. The latter change is motivated by the need to reduce multiple Coulomb scattering. The rectangular geometry is more favorable for tiling a large area, as we envision for the RICH detector at the SSC.

2.7.2 Prototype Detector with Smart-Pad Readout

The smart-pad chamber concept has been developed to obtain a low-cost unambiguous, two-dimensional readout of detectors in a high-multiplicity environment, such as that found at the RHIC and the SSC [13, 14, 15]. The name *smart-pad chamber* is applied to wire chambers that have a cathode plane segmented into a grid of resistively connected pads. The consequent charge sharing among pads permits good resolution even when only every nth pad is read out. Resolutions of 100 μm have been achieved with 1-mm pads with only 1 in 6 being read out (but with the smart-pad technique using only one coordinate).

The smart-pad technique offers the prospect of affordable large-area Ring-Imaging Čerenkov (RICH) detectors, needed at the SSC for hadron identification in the study of B physics.

We plan to build smart-pad chambers using an evaporation technique to deposit the resistors. This is a quick and reliable method used by others. Initially, the goal will be to compare the simulation work of R. Palomera-Garcia (see Sec. 5.1) to actual measurements.

3 Progress Report - Fermilab

3.1 Introduction

Significant progress has been made in the last year at Fermilab. The activities have been characterizing the basic properties of the photocathode. Aging is now much better understood, and in fact is no longer a major problem, though more work is required for operation at the SSC. Other properties of the photocathode, such as a high quantum efficiency and beneficial effects of heating, have been confirmed. Finally, recent work is confirming the excellent timing properties of the solid photocathode.

Summaries of this work is presented in preprints attached to the end of this proposal. In the following we briefly introduce this work.

3.2 Status Report, July 1991

This note summarizes the work of B. Hoeneisen in the 1990 and outlines the plan for 1991.

3.3 Progress Report, August 1991

This note reports the discovery that heating of the photocathode was very beneficial in reducing aging.

3.4 Technical Memo on Aging, September 1991

This memo sets forth the hypothesis that there are four phenomena associated with CsI-TMAE photocathode aging:

1. Adsorption of water by the photocathode.
2. Charging of the photocathode.
3. An unidentified reversible process of aging; the recovery rate increases with increased temperature.
4. An unidentified irreversible process (perhaps migration of Cs off the cathode).

4 Progress Report - Princeton

4.1 Creation of a Photocathode-Fabrication Facility

Inspired by the work of the Anderson group [3, 4, 5], and by the Charpak group [6, 7, 8] that high quantum-efficiency UV photocathode can be readily made by

adsorbing TMAE on thin semiconductor films, we have sought to participate in this exciting field. Our first step was the construction of a small photocathode-fabrication facility. This is based on a (used) Denton DV502 evaporator, equipped with a Sycon STM-100 thickness monitor. Because TMAE, as well as Cs and I readily contaminate the evaporator from the point of view of other users, it seemed prudent to construct our own dedicated facility. D. Anderson kindly provided us with a sample of cleaned TMAE sufficient for several years of operation.

We can now produce a photocathode in about one hour, of sizes up to about 8 inches in diameter. In addition to making the photocathodes for our own use, we have been able to provide the large, quarter-circle photocathode sections for the U. Pennsylvania RICH prototype.

4.2 Photocathode Test Set-up

To study the quantum efficiency of the photocathodes we have adopted a clever technique of B. Hoeneisen [4] that permits comparison of the test photocathode with that of TMAE gas, which has been well studied [16].

The apparatus is shown in Fig. 18. The flat photocathode is separated from an 80%-transparent wire-mesh anode plane by 1.6 mm, forming a parallel-plate avalanche chamber. When the chamber is filled with, say 20-torr of CH_4 gas, gains of 10^5 are readily achieved with a 600-volt potential, and signals from single photo-electrons can be detected.

The chamber can also be filled with a mixture of CH_4 and TMAE gas, and UV photons converted in an 18-mm gap. The conversion electrons are pulled by a weak electric field into another 1.8-mm gap where gain occurs. By comparison of the rates observed using the solid photocathode with those using the TMAE gas, the relative quantum efficiency of the solid photocathode is determined. Then using Ref. [16] for the absolute quantum efficiency of TMAE gas, the absolute quantum efficiency of the solid photocathode is determined. Unlike in Ref. [4], the gain gap for the TMAE-gas operation is different from that for the solid photocathode, so that any aging of the latter will not influence the normalization to the response of the TMAE gas.

The rest of the apparatus consists of a deuterium lamp and a monochromator. In the future we plan also to use a hydrogen lamp (designed by D. Anderson) that emits 3-ns-wide pulses rather than the continuous beam of the deuterium lamp. Our monochromator should be replaced by a double monochromator as the stray light contamination in the present setup is at the percent level.

4.3 'Sponge' Photocathodes

A major emphasis of our studies of photocathodes will be to explore the utility of spongelike materials obtained by evaporating the semiconductor in the presence of TMAE vapor. This approach is motivated by work in the television [17] and x-ray

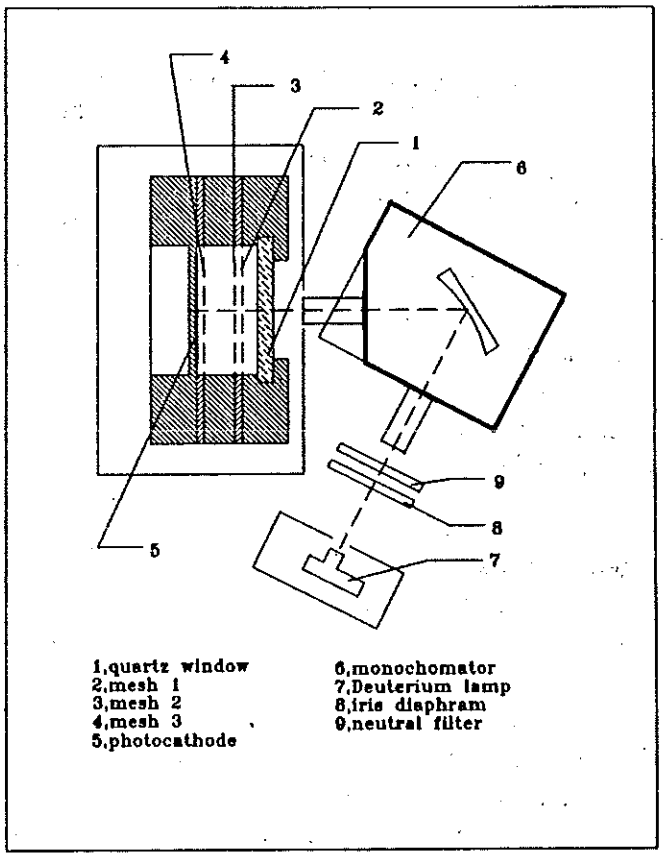

Figure 18: The photocathode test set-up that permits comparison of the quantum efficiency of a solid photocathode with that of TMAE gas.

imaging [18] industries. They found that cathodes of KCl and CsI have enhanced electron transport efficiency if the cathodes are made in an atmosphere of a few torr of argon. The resulting cathodes have density only about 5% of ordinary KCl or CsI, and appear to have significantly longer scattering lengths (in gm/cm^2) for eV electrons than do the dense forms of these materials.

A CsI-TMAE sponge could have two advantages over a CsI + adsorbed TMAE photocathode.

1. The photoabsorption length of TMAE is only 10-20 molecules. In a CSI + adsorbed TMAE cathode there is (presumably) only a single layer of TMAE on the surface, so that TMAE layer can contribute at most 5-10efficiency of TMAE gas; the rest must come from the CsI substrate. However, in a 'sponge' photocathode many more than 20 layers of TMAE molecules can be trapped, so the cathode should achieve (at least) the quantum efficiency of TMAE gas. Indeed, the other material need not be CsI, but can be any material that is transparent to UV photons. Since CsI cathodes have aging that may be problematic in some applications [5], the use of another host material may provide a superior photocathode. We expect that the 'sponge' photocathodes will achieve full quantum efficiency in layer perhaps only 100 molecules thick.

2. The 'sponge' cathodes may prove to have superior detection efficiency for charged particles. This could be relevant for application to large-area, very thin time-of-flight counters. For example, a minimum ionizing particle deposits about (1.5 $MeV/gm/cm^2$) (4.5 gm/cm^3) (10^{-4} cm) = 700 eV in a 1-μm thick layer of CsI. Then assuming it takes 30 eV to liberate on electron there would be about 20 electrons ionized by the passing particle. But there appears to be poor electron transport in a 1-μm layer is CsI. If this is significantly improved in the 'sponge' cathodes, large signals could be obtained in very thin layers. Then if only the very fast electron component of the pulse in the parallel-plate chamber is used, excellent time resolution should be obtainable for single particles.

We propose to investigate these two aspects of 'sponge' cathodes in great detail in FY92.

We have made a preliminary comparison of the sensitivity to cosmic rays of an ordinary 1-μm-thick CsI + TMAE cathode to a 'sponge' cathode containing the same amount of CsI, but only 1/20 the density. We found the rate of detection of cosmic rays in the 'sponge' cathode to be twice as high as in the ordinary cathode. We have not yet determined the absolute efficiency of detection of minimum ionizing particles by these cathodes.

4.4 Photocathodes for Dense Scintillators

Some of the early interest in TMAE photocathodes was for its potential application to viewing the UV light from a dense scintillator such as BaF_2 [19]. However, only

about 50% of the fast component of the BaF_2 scintillation light overlaps the quantum efficiency of TMAE. A much better match is liquid xenon, whose scintillation spectrum peaks at 170 nm [20], and has a decay constant of less than 3 ns.

We also propose to explore the use of solid TMAE-based photocathodes in liquid xenon in FY 92. The proposed test chamber is shown in Fig. 19, based on the design of Ref. [21]. We must also build a cryostat and purification/recirculation system for the liquid xenon along the lines described in Ref. [22].

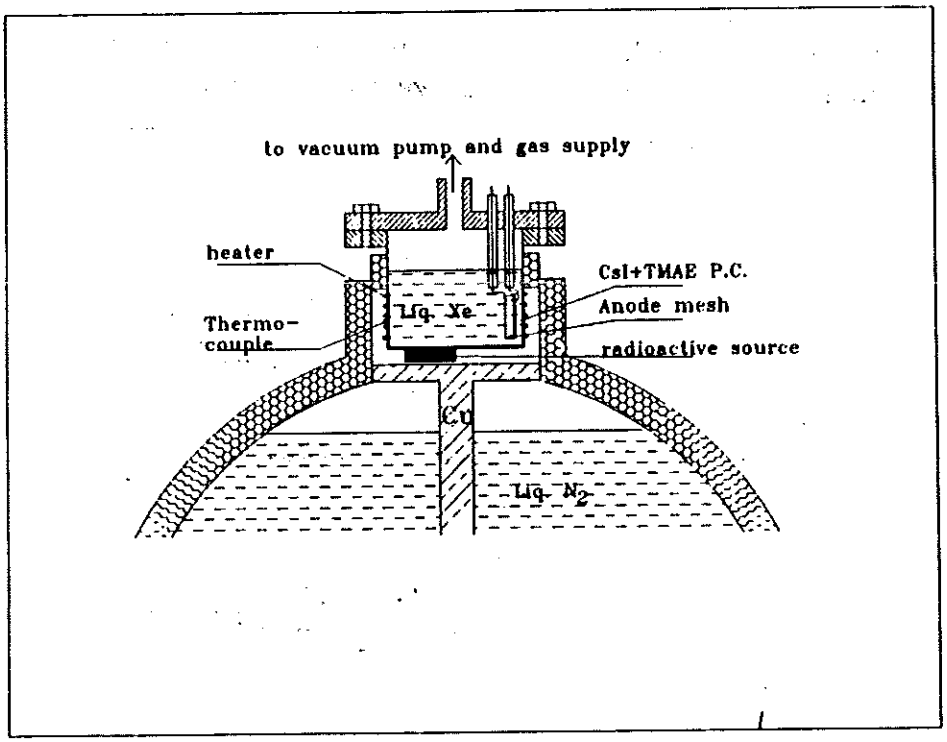

Figure 19: Proposed liquid-xenon test chamber.

We will suspend the photocathode directly in the liquid xenon, avoiding any attenuation of light in an optical window. To guarantee good signal-to-noise, we will couple the photocathode to a wire-mesh (or parallel-wire) anode plane separated by 1.6 mm, and operate the chamber with a gain of 10-100. Among the noble liquids, only xenon shows promise for use as a gain medium [23]. In our chamber the drift time of the photoelectrons will be about 500 ns, but there will be little dispersion in this drift time (unlike for an ionization chamber). Thus the parallel-plate chamber could provide both gain and analog storage, while maintaining the excellent time resolution of xenon scintillation light.

5 Progress Report - Puerto Rico

5.1 Simulation with SPICE

A model of the two-dimensional smart-pad chamber has been constructed using CADENCE and SPICE. This work is being done by Professor R. Palomera-Garcia, of the Electrical Engineering School at the Universidad de Puerto Rico. The pad array is represented by capacitors to ground that are interconnected by resistors. The capacitance chosen for the initial studies is 3 pf per pad, and the resistance is varied between 2 and 10 kΩ. The amplifiers are presently ideal and are simulated by a 300-Ω load. The study will initially determine the optimal placement for the amplifiers for our application, the resistor configuration and the associated charge sharing at each node. Fig. 20 shows a possible placement for the resistors and amplifiers in a unit cell.

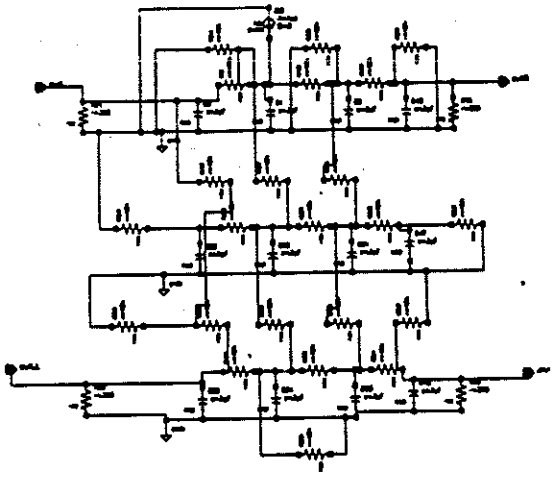

Figure 20: Possible resistor and amplifier placement for a smart-pad chamber.

In the simulation, an input pulse has been injected into the array and the signal on each of the amplifiers is then studied. This information along with the expected noise floor of the amplifier and the signal size will help determine the type of pad configuration we will build and test. This simulation is simple and the results are returned quickly. Measurements of the charge distribution on the pads from Fe^{55} can be used as input for the simulation. The resulting distribution of charge in the amplifiers can then be compared to the model.

5.2 Proposed Research

The proposed R&D program at Puerto Rico has the following goals:

- The SPICE simulation work will continue to help us understand the behavior of chambers and the amplifier. We intend to compare the model with measurements and be able to predict the spatial resolution and the ability to identify two hits.
- Simulate the preamplifier design of C. Britton with SPICE and optimize the design for use with a resistive and capacitive circuit, such as that of the smart-pad chamber.
- Submit a prototype preamplifier design to MOSIS and make preliminary tests of the device at Puerto Rico. This would be followed with tests of the chip using a smart-pad chamber provided by Pennsylvania.
- Analyze data from the test-beam run this fall at Fermilab of the Pennsylvania prototype RICH chamber.

6 Progress Report - Oak Ridge

6.1 Overview

Figure 21 illustrates the proposed RICH-pad readout-chip architecture. Versions of the basic functional blocks of this chip have already been designed, fabricated in 2-μm CMOS, and tested. Several versions of the preamplifier for capacitive pad readout have been fabricated and tested. Two versions of the analog memory, a 16×1 and a 16×4 version, have been designed and fabricated and are presently in test. Two versions of the ADC have been fabricated and are being tested. The entire architecture is intended to be run at approximately 112 ns per event. Extending this to a 160-ns event rate should prove quite feasible.

6.2 Preamplifier

The preamplifier design shown in Figure 22 was designed for capacitive pads having values of 10-50 pf. The risetime is approximately 25 ns for 25-pf pad capacitance and the power dissipation is approximately 4.5 mW.

Since our actual detector presents more specific values of capacitances, this preamplifier design might be customized. This should ease actual system integration since much experience has been gained from this present design and since good versions of remaining parts of the chip have been designed for this front end.

6.3 Correlated Sampler and Analog Memory

Assuming the data collection is synchronous, a correlated sampler is more suitable than conventional time-invariant shaping and peak detection. We have designed two correlated samplers, one of which is shown in Fig. 23. The first has been fabricated

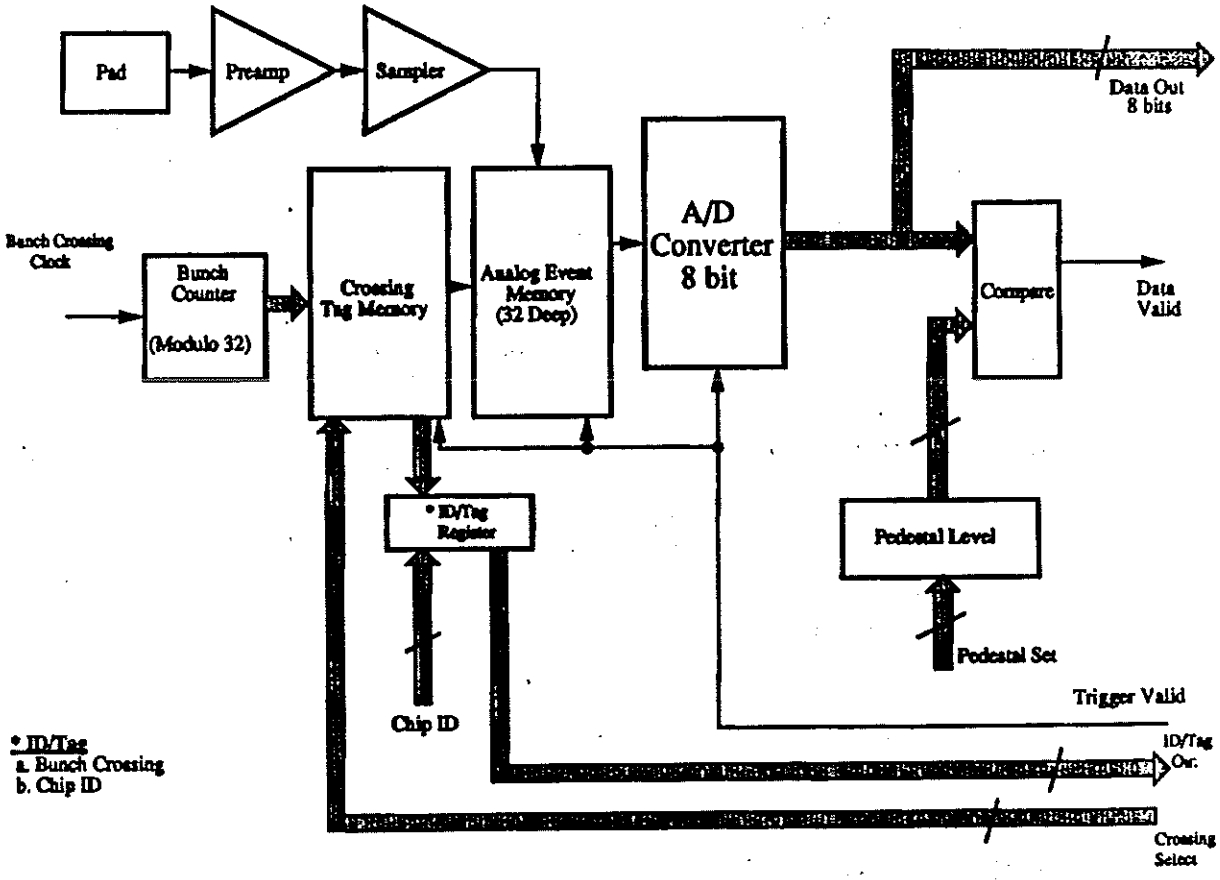

Figure 21: RICH-pad readout-chip architecture.

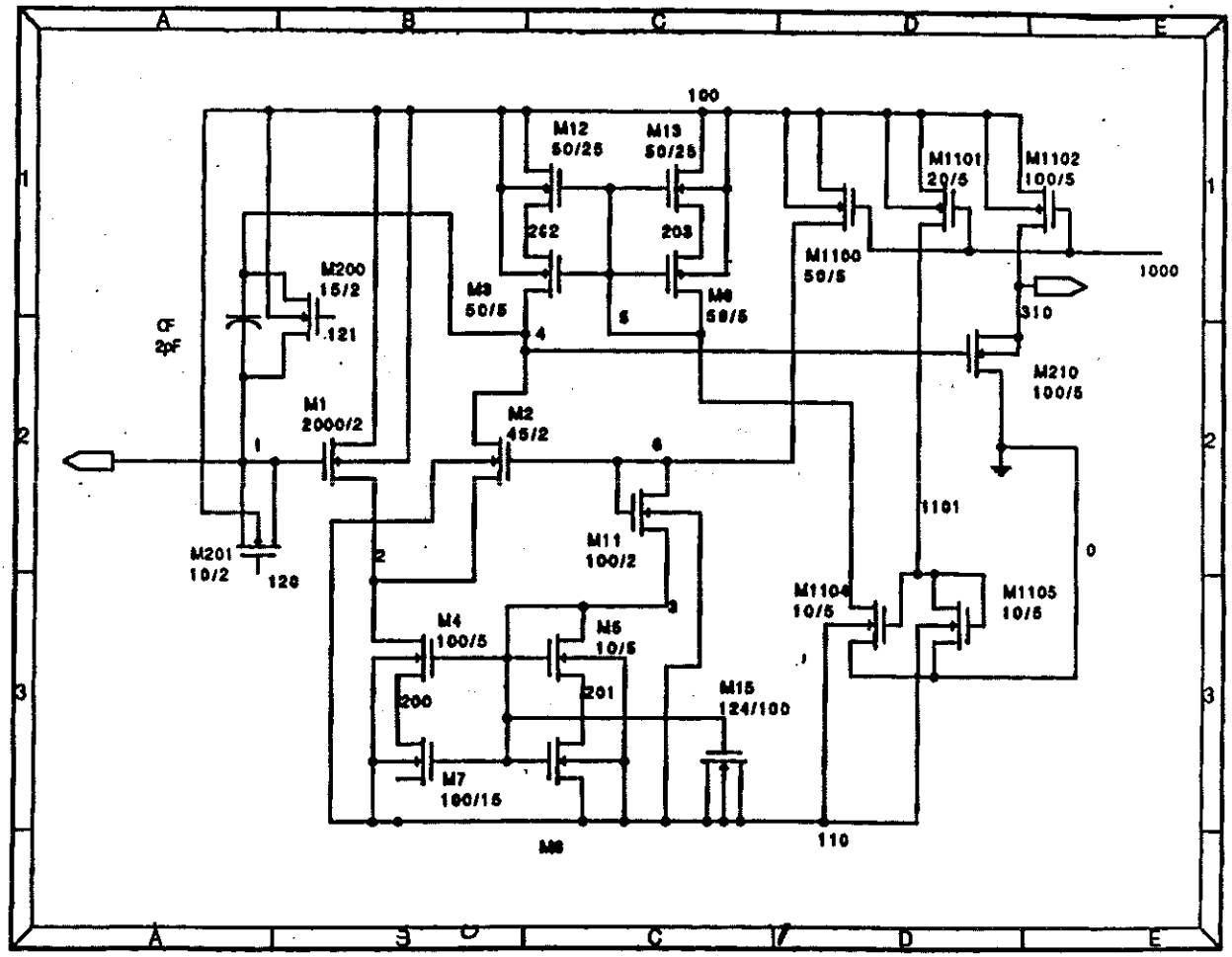

Figure 22: Preamplifier design for pads.

and tested, and the second, improved and simplified design will be submitted for fabrication shortly.

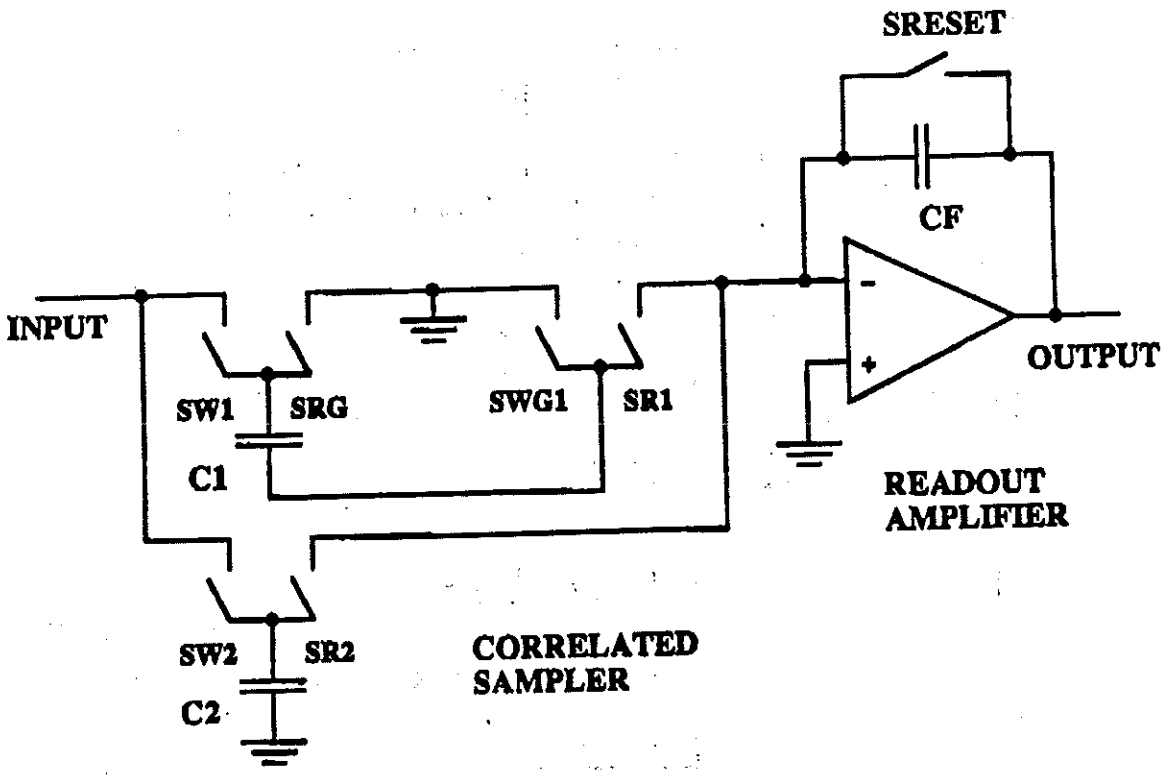

Figure 23: Correlated Sampler.

An analog memory compatible with the correlated sampler has also been designed and fabricated and is shown in Figure 24. It uses 1-pf capacitors as storage elements and is designed for writing at the event rate with readout taking place simultaneously at a lower rate. Preliminary testing at an event rate of 1 MHz gave the linearity curve shown in Figure 25. For this data, reading and writing took place at the same rate with the read address offset by 8 from the write address. We think this basic architecture could be used for the RICH application. Should it be necessary, the memory depth could be doubled with only minor modifications. We are still evaluating the linearity and dynamic range of the memory. The RICH requirements would need to be compared to those results and the memory improved if needed.

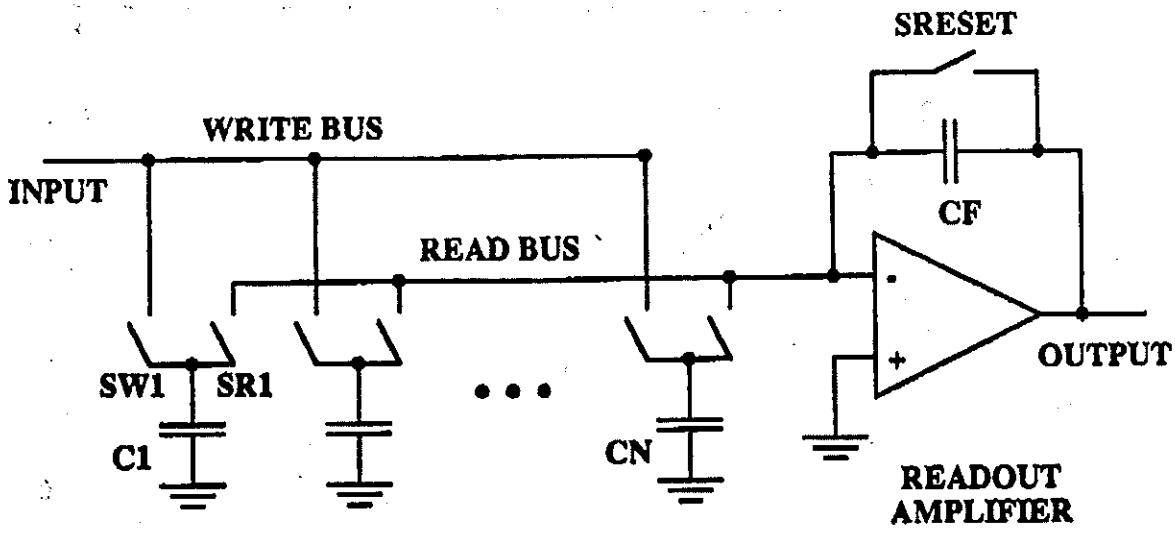

6.4 ADC

An 8-bit, successive-approximation A/D Converter has been designed and fabricated and is presently in test. The goal is to develop a converter that is expandable from 8 to 10 bits with a conversion time of approximately 5-10 μs using system clocks of 112 ns. The present design has a differential linearity of approximately 1/2 LSB. We would customize the resolution and readout format for the RICH application. Should more than 10 bits be necessary, we would continue development of a Wilkinson converter. This would be slower than the successive-approximation approach, but would allow better resolution.

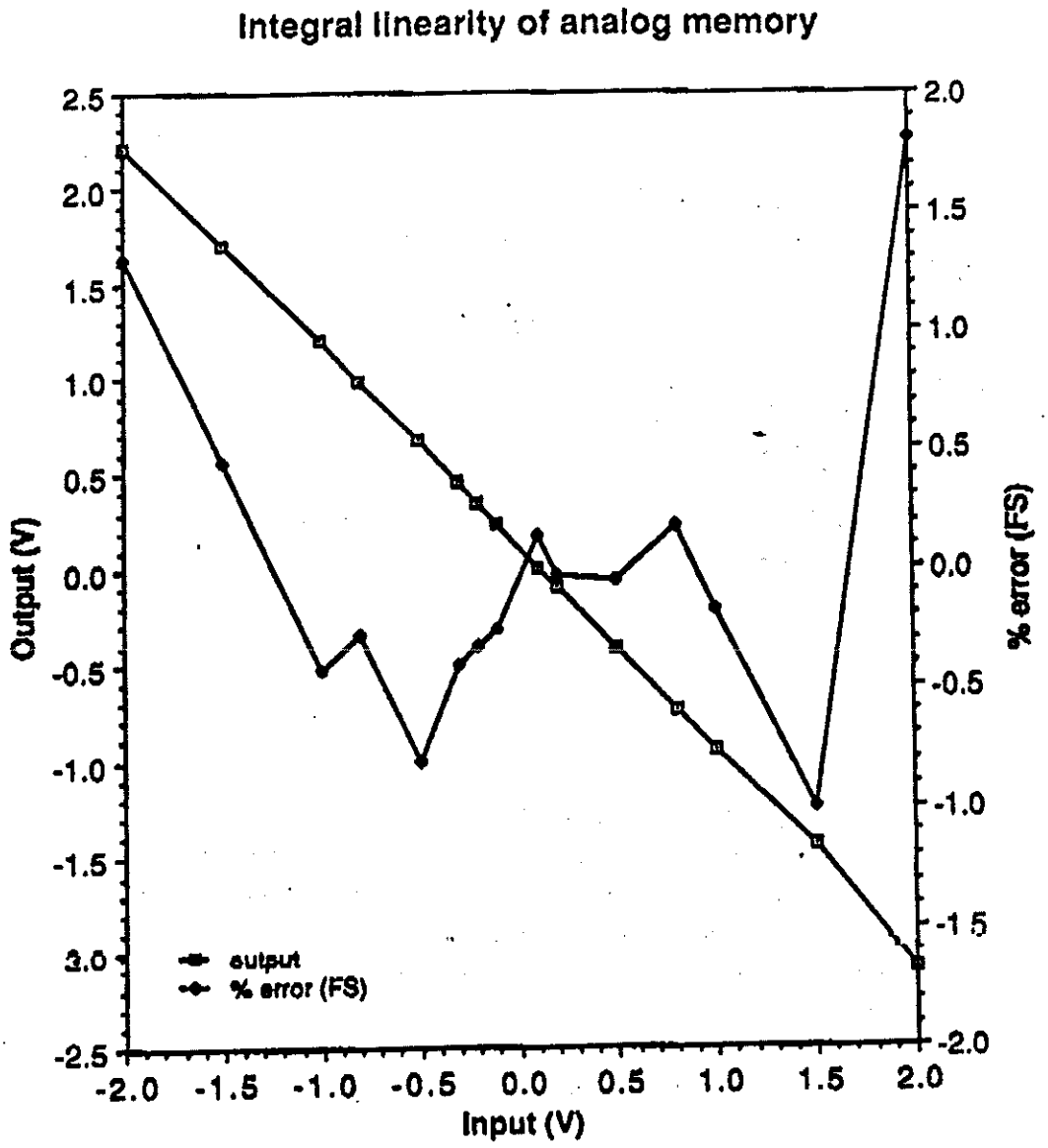

Figure 25: Analog-Memory linearity.

7 Budget Proposal for FY92

7.1 Fermilab

In FY92 we will continue studies of the solid photocathode. The salary of S. Kwan is paid by Fermilab. We request funds for the salary of B. Hoeneisen (Electrical Engineer) for the summer months. In addition, we request funds to build a combined time-of-flight and RICH detector at Fermilab. J. Morfin will direct this project. We request funds to build a test prototype chamber.

1. Permanent Equipment

    1. CAMAC and NIM modules: 12-channel ADC, Dataway Display, I/O Register, QVT and CAMAC interface, Octal Discriminator, 4-Fold Logic Unit, NIM bin and power supply $10k
    2. 2 Droege positive H.V. supplies $1.5k
    3. Vacuum pump $1.5k
    4. Gas-handling equipment $10k
    5. Control and readout electronics for SVX chips $25k
    6. Electronic test equipment $20k
    7. PC-clone computer for data acquisition and offline analysis $5k

    Total Permanent Equipment $73k

2. Materials, Supplies, and Travel

    1. Gases $2k
    2. Quartz windows $2k
    3. Pad planes (bakeable, vacuum tight, inert, double-sided) $5k
    4. Other materials for chambers $3k
    5. Travel (Between FNAL, Quito and Dallas $10k

    Total Materials, Supplies, and Travel $22k

    Indirect costs of 36% on item 2 ..... $7k

3. Salaries

    1. Three-month salary of B. Hoeneisen (Electrical Engineer) $25k

    Total Salaries $25k

4. **Total Fermilab Budget $115k**

7.2 Oak Ridge

In FY92 we will design, fabricate and test a single I.C. that contains a preamplifier, buffering, and an ADC that runs with a 160-ns clock frequency, appropriate for a B detector at the SSC.

1. Permanent Equipment

Total Permanent Equipment $0.0k

2. Materials, Supplies, and Travel

    1. Operating funds for travel, publications, and MOSIS submissions .. $10k

Total Materials, Supplies, and Travel $10k

Indirect Costs of 67% on Materials, Supplies, and Travel $7k

3. Salaries

    1. C. Britton (Electrical Engineer) $20k

Total Salaries $30k

Indirect Costs of 67% on Salaries $13k

Total Indirect Costs of 67% $20k

Total Oak Ridge $50k

7.3 University of Pennsylvania

In FY92 we will continue studies of the present prototype RICH detector. We envision several improvements to the present design that would be of interest. First, the present pad plane can be replaced with a 1-D and then 2-D smart pad plane. This requires the purchase of an evaporator. A second hand machine will be adequate. The TMAE vapor is very sticky and the evaporator requires thorough cleaning after each evaporation. Consequently, the condensed matter physicists quickly realize they do not want TMAE in their evaporator. This past year, we drove to Princeton, but that was most inconvenient since we must carry our vacuum vessels with us.

Second, we would like to employ a window design that maximizes the surface area of the chamber. Third, we would like to build a new interface board that results in a better vacuum seal at the point where the signals emerge from the vacuum. Four, we will to design and build a detector using composite material rather than stainless steel for the outer shell. Five, redesign the printed circuit board that presently uses the SVX and use the 16-channel readout system from Oak Ridge.

1. Permanent Equipment

    1. Composite material test chamber $5k
    2. Used Evaporator, with bell jar and thickness monitor. $10k
    3. 16-CFM vacuum pump, Leybold Model-D16B $2k
    4. Nitrogen container $1k
    5. 2 Type 600 Barocel Pressure Transducers $2k
    6. Hydrogen lamp (Hamamatsu) $2k
    7. Two positive High-voltage power supplies (Bertan 377) $4k
    8. NIM electronics: Power Supply for crate, quad discriminator, quad coincidence, gate generator, quad BCD scalar $10k
    9. CAMAC electronics: 12-channel ADC, Dataway Display, and an I/O Register $8k
    10. Ortec preamp, shaping amplifier, and multichannel analyzer $5k
    11. Cleanbench $3k
    12. Four PMT's for cosmic ray telescope $4k
    13. DMM/Picoammeter $2k
    14. Postscript Printer $3k

Total Permanent Equipment $61k

2. Materials, Supplies, and Travel

    1. Stainless-steel fittings, tubing, valves, *etc.* $5k

2. High-purity chamber gases $2k
3. Operating funds for travel, publications, and miscellaneous supplies $10k

Total Materials, Supplies, and Travel $17k

Indirect Costs of 67% on Materials, Supplies, and Travel $11k

3. Salaries

1. J. Millan (Electrical Engineering Ph.D. candidate) 50% Tuition $10k
2. J. Millan (EE) $1k stipend per month $9k

Total Salaries $19k

Indirect Costs of 67% on Salaries $13k

Total Indirect Costs of 67% $24k

Total University of Pennsylvania $121k

7.4 Princeton University

In FY92 we will explore the fabrication and use of novel photocathodes made from low-density 'sponges' of TMAE and semiconductors such as CsI and CuI. We will evaluate these photocathodes for use in Čerenkov counters as well as in calorimeters based on high-density scintillators, particularly liquid xenon. We will also evaluate these materials as direct sensors of charged particles, for use in time-of flight systems.

1. Permanent Equipment

1. Stainless-steel test chamber $5k
2. Double monochromator (Instruments SA, DH-20) $3k
3. 10-CFM vacuum pump $2k
4. Pressure sensors $2k
5. Hydrogen lamp (Hamamatsu) $2k
6. High-voltage power supplies (two Bertan 377) $4k
7. Stainless-steel gas regulators $1k
8. Optical bench $1k
9. NIM electronics: crate, hex discri, quad coincidence, gate generator, counter/timer, TAC, constant-fraction discri $10k
10. PC-clone computer $5k
11. Cryostat for liquid xenon $10k
12. Xenon purification and recirculation system $15k
13. Stainless-steel test chamber for liquid xenon $5k
14. Pressure and temperature monitors $3k
15. Low-noise preamplifier (EG&G 142PC) $1k
16. Shaping amplifier (EG&G 570) $1k
17. Multichannel analyzer (EG&G Ace 8k) $3k

Total Permanent Equipment $73k

2. Materials, Supplies, and Travel

1. Stainless-steel fittings, tubing, valves, *etc.* $5k
2. High-purity chamber gases $2k
3. Liquid xenon (1 liter) $3k
4. Operating funds for travel, publications, and miscellaneous supplies $10k

Total Materials, Supplies, and Travel $20k

Indirect Costs of 67% on Materials, Supplies, and Travel $13k

3. Total Princeton University $106k

7.5 Puerto Rico

In FY92 we will simulate and submit through Oak Ridge a fabrication of a tiny chip preamplifier that optimizes the features needed for a smart-pad resistive and capacitive network. We request support for travel and subsistence for A. Lopez and Palomera-Garcia and a Sun IPC workstation for A. Lopez to carry out the data analysis and simulation work.

1. Permanent Equipment

1. Sun IPC workstation with 16-inch color monitor.....$6k.

Total Permanent Equipment.....$6k

2. Materials, Supplies, and Travel

1. Operating funds for travel to Fermilab and Pennsylvania for A. Lopez and graduate students.....$15k
2. Travel and subsistence for Palomera-Garcia to work at Oak Ridge for the summer.....$5k.

Total Materials, Supplies, and Travel.....$20k

Indirect Costs of 67% on Materials, Supplies, and Travel.....$13k

3. Salaries

1. Summer Salary for Palomera-Garcia.....$10k.

Total Salaries.....$10k

Indirect Costs of 67% on Salaries.....$6k

Total University of Puerto Rico.....$53k

8 Personnel

8.1 Fermilab

B. Hoeneisen will spend 100% time during the summer on this project. S. Kwan spends 50% time on this project. J. Morfin will direct the prototype building and spend 25% on this project.

8.2 Oak Ridge

C. Britton will spend 20% time on this project.

8.3 University of Pennsylvania

In the past year, J. Millan worked 100% time on this project. This coming year he will attend Penn as a graduate student in Electrical Engineering. His research will continue to be the RICH detector. J. Millan will work 50% time on R&D for this RICH proposal. S. Peil will perform his undergraduate thesis project on the smart pad work. N. Lockyer will spend about 25% time on this project. In addition, Penn provides support at no cost to the project in the form of about 0.5 FTE technician.

8.4 Princeton University

J.G. Heinrich and C. Lu will work full time on R&D for SSC subsystems. K.T. McDonald will spend 90% of his research time in these projects. Graduate students W.S. Anderson, Y. Zhu, and one other to be named shortly will devote all their research effort to this project. Undergraduate student E. Dunn perform a senior-thesis project on photocathodes in academic year 91-92. In addition, we benefit from access (at no cost to the SSC) to the technical staff of the Princeton High Energy Physics group which includes 1 mechanical engineers, 3 mechanical technicians, 1 electrical engineer, and 3 electrical technician. All salaries of the above people are supported by the DoE HEP Division, except for K.T. McDonald (academic year salary from Princeton University), and W.S. Anderson (NSF Predoctoral Fellow).

8.5 Puerto Rico

The groups at Puerto Rico in the last year have addressed two areas of R&D. Professor A. Lopez (Physics Department) has directed the writing of the software for the readout of the Pennsylvania prototype chamber. In addition, Monte Carlo simulations of the chamber and basic RICH features were written to aid in chamber design. J. Millan performed a Master-thesis project on the construction and testing of a prototype RICH detector. J. Millan was located at Pennsylvania for most of this work. A. Mendez is a graduate student and wrote the online data acquisition program for

the prototype chamber used at Pennsylvania and in the M-Test beam at Fermilab. Some of the work by Mendez was performed at Pennsylvania. C. Hernandez is a graduate student and wrote a simple RICH Monte Carlo program. A. Lopez will devote 30% of his research time to RICH development and the two graduate students will work full-time on the SSC R&D RICH. Most attention will be the analysis of the data from the beam test coming up in a few weeks and data from subsequent prototypes.

Professor R. Palomera-Garcia (Electrical Engineering Department) has spent the last two summers at Oak Ridge working in H. Brashear's group with G. Alley and C. Britton. The main work involved a Spice simulations of a CMOS circuit design for a RICH readout preamplifier and the Spice simulation of the proposed resistive-pad chamber. R. Palomera-Garcia has received two semesters release time from the University of Puerto Rico to work on the SSC R&D RICH project. R. Palomera-Garcia will optimize the preamplifier design of C. Britton for the resistive pad readout. Prototypes will be made and preliminary testing will take place at Puerto Rico.

References

[1] T. Ferbel, *Experimental Techniques in High Energy Physics*, (Addison-Wesley, Menlo Park, CA, 1987) 371-461.

[2] T. J. Gourlay *et al.*, *Proceedings of the Symposium on Particle Identification at High Luminosity Hadron Colliders*, FERMILAB, April 5-7, 89.

[3] D.F. Anderson, *Extraction of Electrons from a Liquid Photocathode into a Low-Pressure Wire Chamber*, Phys. Lett. **118B**, 230 (1983).

[4] B. Hoeneisen *et al.*, *A CSI-TMAE Photocathode with Low-Pressure Readout for RICH* FERMILAB-Pub-90/182 (Sept. 1990), submitted to Nucl. Instr. and Meth.

[5] S. Kwan and D.F. Anderson, *A Study of the CsI-TMAE Photocathode*, FERMILAB-Pub-91/98 (May 1991), submitted to Nucl. Instr. and Meth.

[6] V. Peskov *et al.*, *Liquid and Solid Organic Photocathodes*, Nucl. Instr. and Meth. **A269**, 149 (1988).

[7] J. Séguinot *et al.*, *Reflective UV Photocathodes with Gas-Phase Electron Extraction: Solid, Liquid, and Adsorbed Thin Films*, Nucl. Instr. and Meth. **A297**, 133 (1990).

[8] G. Charpak *et al.*, *Investigation of Operation of a Parallel-Plate Avalanche Chamber with a CsI Photocathode Under High Gain Conditions*, CERN-PPE/91-47 (Feb. 1991).

[9] V. Dangendorf *et al.*, *An X-Ray Imaging Gas Scintillation Detector With CsI-Wire Chamber UV-Photon Readout*, SPIE 1990 Symposium on Instrumentation in Astronomy (Tucson, AZ, Feb. 1990)

[10] S.K. Dhawan *et al.*, *A Rich MWPC Pad Readout by Using Custom Microplex IC's*, IEEE Trans. Nuc. Sci. **35**, # 1 (1988).

[11] S. Kleinfelder *et al.*, *A Flexible 128 Channel Silicon Strip Detector Instrumentation Integrated Circuit with Sparse Data Readout*, IEEE Trans. Nucl. Sci. **35**, 171 (1988).

[12] F. Kirsten and C. Haber, *A Versatile, Programmable Control and Data Acquisition System for Complex Integrated Circuits*, IEEE Trans. Nuc. Sci. **37**, 288 (1990).

[13] A.L.S. Angelis *et al.*, *Test Results with a Novel High-Resolution Wire Chamber with Interpolative Pad Readout*, Nucl. Instr. and Meth. **A283**, 762 (1989).

[14] R. Debbe *et al.*, *A MWPC with Highly Segmented Cathode Pad Readout*, Nucl. Instr. and Meth. **A283**, 772 (1989).

[15] R. Debbe *et al.*, *A Study of Wire Chambers With Highly Segmented Cathode Pad Readout For High Multiplicity Charged Particle Detection*, IEEE Trans. Nuc. Sci. **37**, # 2 (1990).

[16] R.A. Holroyd *et al.*, *Measurement of the Absorption Length and Absolute Quantum Efficiency of TMAE and TEA from Threshold to 120 nm*, Nucl. Instr. and Meth. **A261**, 440 (1987).

[17] G.W. Goetze *et al.*, *Field-Enhanced Secondary Electron Emission from Films of Low Density*, J. Appl. Phys. **35**, 482 (1964).

[18] J.E. Bateman and R.J. Apsimon, *A New Photocathode for X-Ray Image Intensifiers Operating in the 1-50 keV Region*, Adv. Elec. and Elec. Phys. **52**, 189 (1979).

[19] D.F. Anderson *et al.*, *Coupling of a BaF_2 Scintillator to a TMAE Photocathode and a Low-Pressure Wire Chamber*, Nucl. Instr. and Meth. **217**, 217 1983).

[20] S. Kubota *et al.*, *Liquid and Solid Argon, Kryton, and Xenon Scintillators*, Nucl. Instr. and Meth. **A289**, 236 (1990).

[21] K. Masuda *et al.*, *Test of a Dual-Type Gridded Ionization Chamber Using Liquid Xenon*, Nucl. Instr. and Meth. **174**, 439 (1980).

[22] E. Aprile *et al.*, *Measurements of the Lifetime of Conduction Electrons in Liquid Xenon*, Nucl. Instr. and Meth. **A300**, 343 (1991).

[23] S.E. Derenzo *et al.*, *Electron Avalanche in Liquid Xenon*, Phys. Rev A **9**, 2582 (1974).

Status report on the development of a fast solid photocathode RICH or TOF.

The device is shown in figure 1. An incident Cerenkov UV photon traverses the quartz window and the anode wire mesh, and releases a single electron from the surface of the solid CsI-TMAE photocathode. This electron drifts towards the anode which is connected to a positive voltage source. The applied voltage is sufficiently high that avalanche multiplication occurs. The induced charge on the cathode pads is amplified external to the detector. The gas is typically methane at 20 Torr, the anode-to-cathode spacing is 1.6 mm, and the anode-to-cathode voltage is approximately 600 V. To obtain a compact detector we use a solid NaF or a liquid C_6F_{14} Cerenkov radiator. "Proximity focusing" (i.e. no focusing) is used for the RICH detector. The achievable pion-kaon separation is shown in figure 2. For the time-of-flight device we place the Cerenkov radiator directly on the quartz window.

The quantum efficiency of the photocathode is shown in figures 3 and 4 as a function of wavelength and ageing. Note that the initial efficiency of approximately 22% can be enhanced to approximately 38% by operating the device initially at a low current density. This efficiency then decreases as a function of the collected charge (i.e charge of the ions that neutralize on the photocathode, or equivalently, the charge of photoelectrons times the gain), and levels out at approximately 16%.

We have obtained gains in the one-step avalanche multiplication between 10^4 and 10^7 depending on cathode-to-anode spacing and gas, see figure 5. We have achieved signal-to-noise ratios for SINGLE photo-electrons as high as 10,000:1. This signal-to-noise ratio is achieved by integrating the ion current which has a duration of order 400 ns. For time-of-flight measurements it is necessary to amplify the fast electronic component of the signal. We have achieved signal-to-noise ratios for SINGLE photoelectrons of 4:1 with the high bandwidth required to see the fast electron component of the signal. For time-of-flight applications it is therefore necessary to have many photoelectrons per particle.

For a time-of-flight system there are three contributions to the time resolution: avalanche multiplication, different Cerenkov photon travel times, and electronic noise. The calculated 1-sigma contributions to the time resolution for typical operating conditions ($G = 10^5$, L = 1.9 cm, 30 photoelectrons) are respectively 12ps, 12ps and 25ps (add in quadrature).

The following steps in the development of practical devices are: i) Study of the ageing mechanism; ii) Proof of principle of the time-of-flight resolution; iii) Obtain the optimum

anode-to-cathode separation for maximum gain; iv) Investigate operation at room pressure by adding helium to the methane.

The ageing problem must be understood and overcome before practical devices can be considered.

Publications:

"A CsI-TMAE photocathode with low-pressure readout for RICH", B. Hoeneisen, D.F. Anderson and S. Kwan, NIM A302 (1991) 447-454.

"A study of the CSI-TMAE photocathode", S. Kwan and D.F. Anderson, submitted to NIM.

Bruce Hoeneisen
7 Aug. 1991

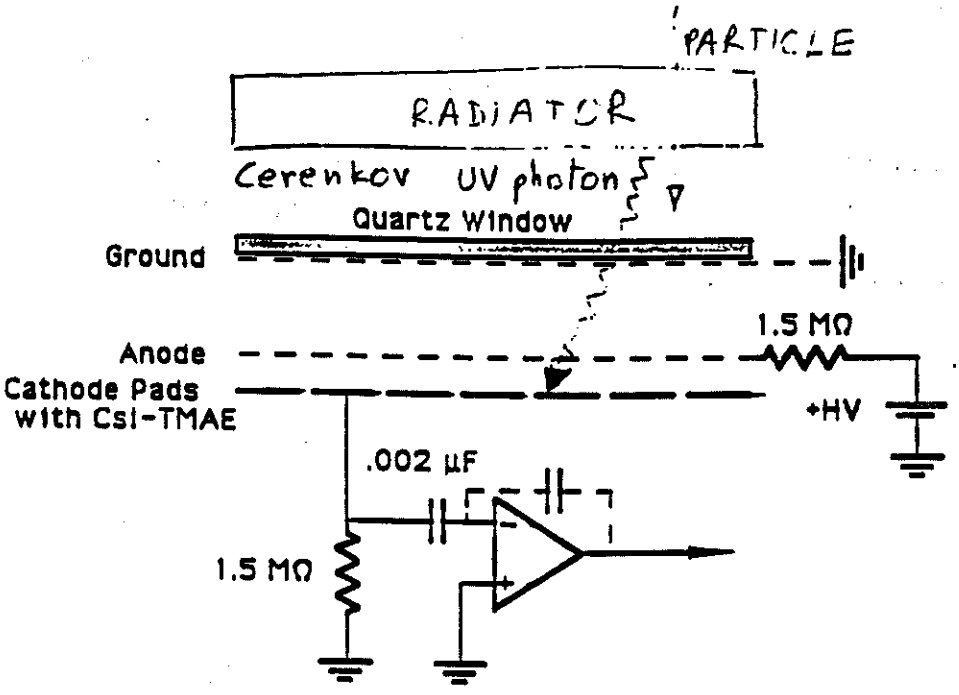

Figure 1. Schematic diagram of the device.

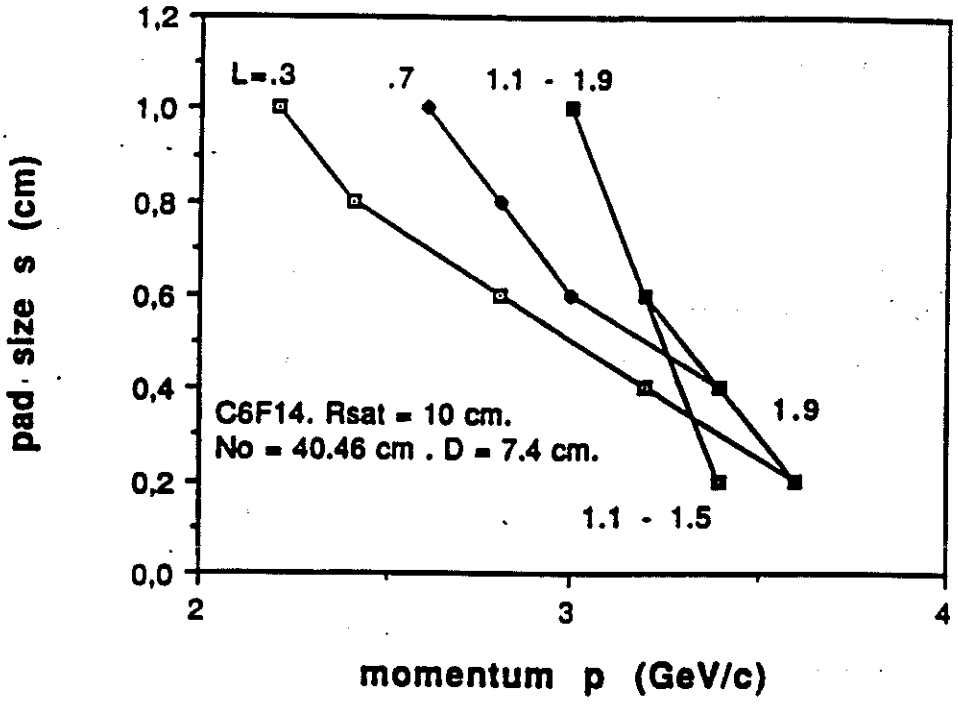

Figure 2. Pion-kaon separation at 95% confidence as a function of pad size for several radiator thicknesses. The photocathode efficiency is assumed to be 10%.

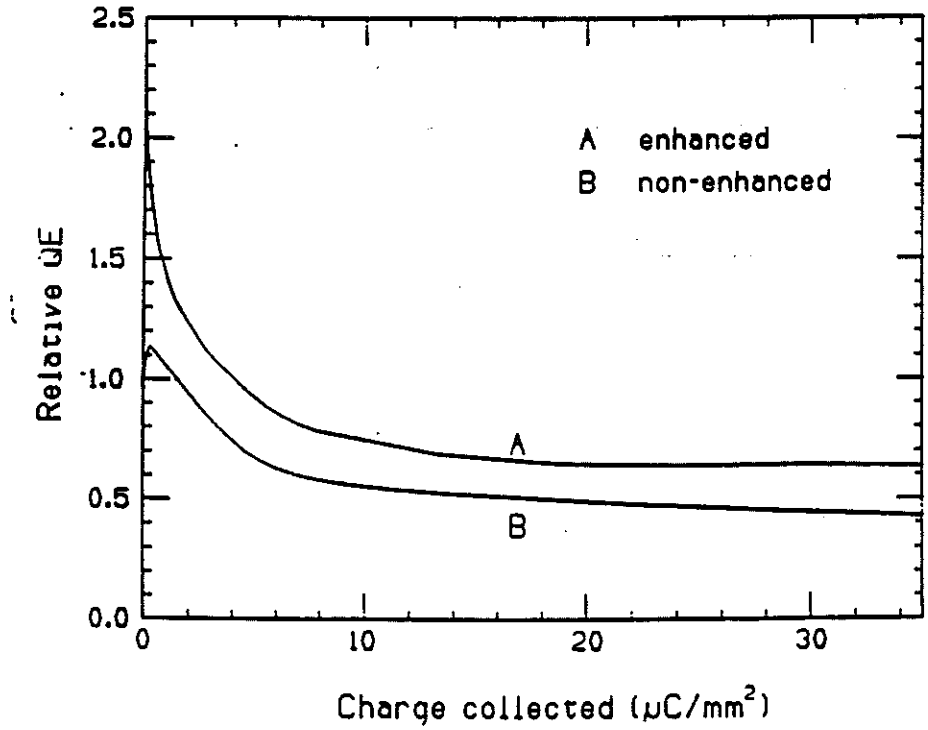

Figure 3. Relative quantum efficiency as a function of the collected ion charge. Note in A the enhancement obtained by initially running at a low counting rate.

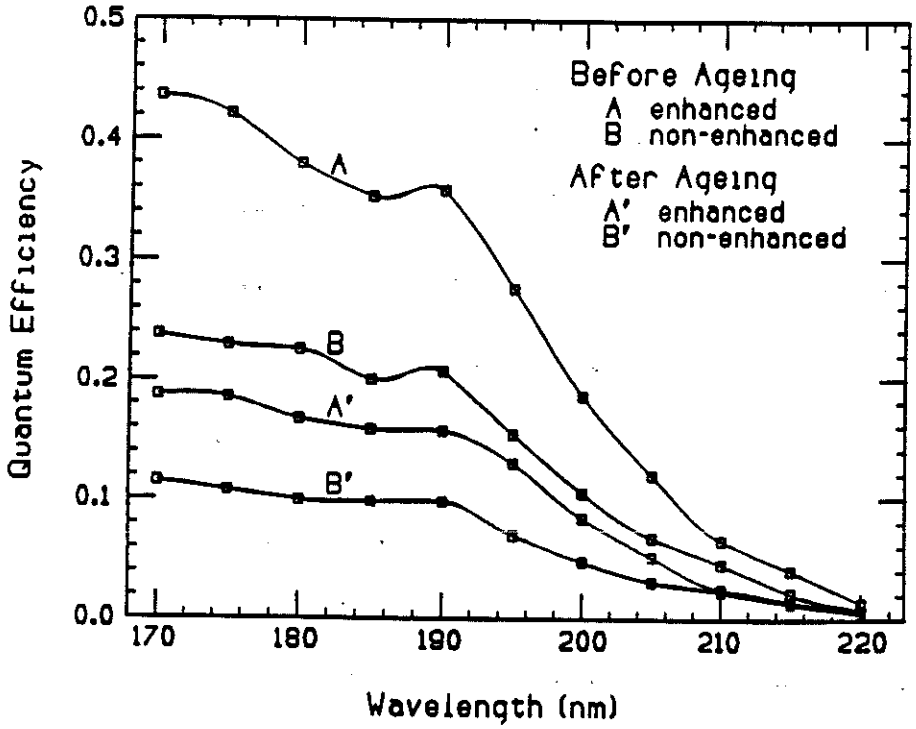

Figure 4. Quantum efficiency of the photocathode as a function of wavelength.

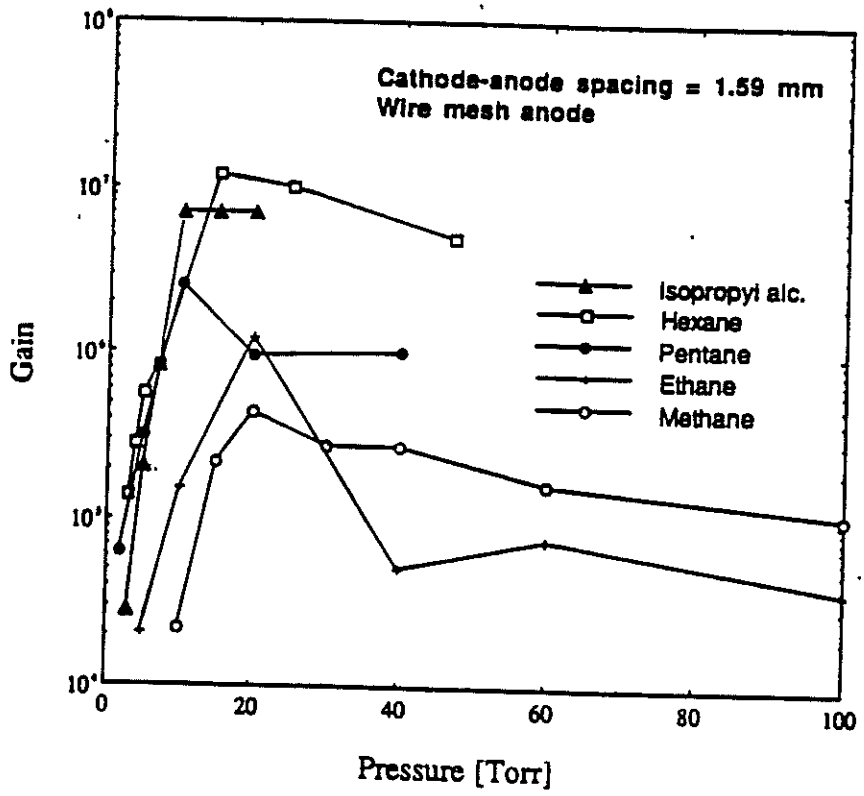

Figure 5a. Maximum gain as a function of pressure for several gases.

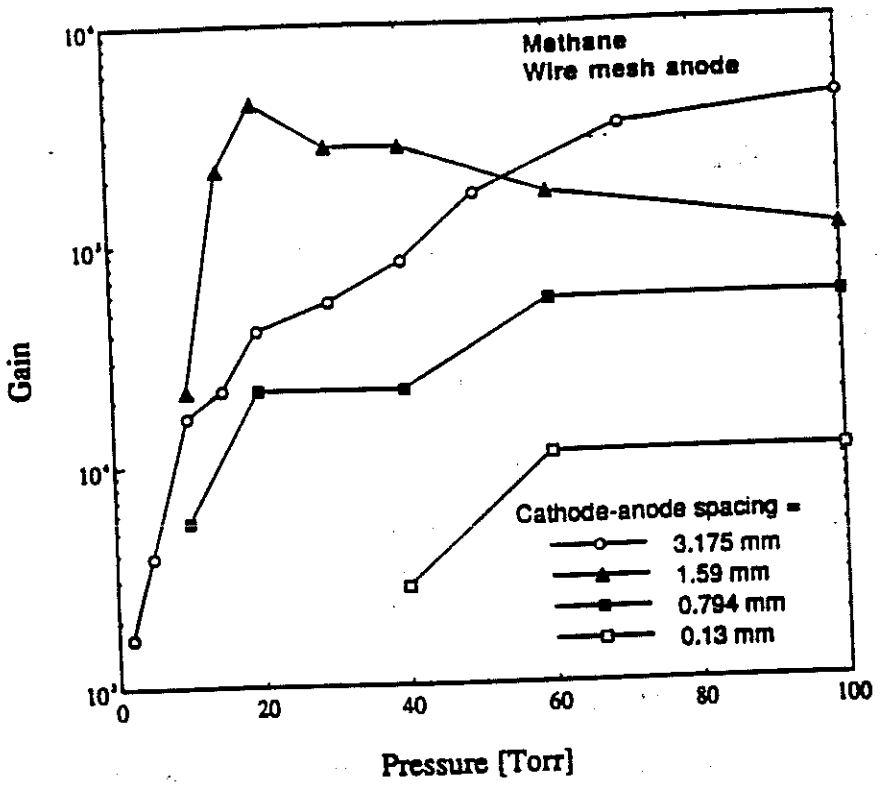

Figure 5b. Maximum gain as a function of pressure for several anode-to-cathode spacings.

Progress report on the development of a solid photocathode avalanche chamber (July and August 1991).

1.- Introduction

Since the summer of 1990 a research effort at FERMILAB has been carried out with the objective of developing a fast imaging UV detector with a solid CsI-TMAE photocathode, low pressure avalanche multiplication, and pad readout. This device may be useful for a fast Ring Imaging Cerenkov detector (RICH), for a time-of-flight detector when coupled to a solid NaF or liquid C_6F_{14} Cerenkov radiator, or a fast calorimeter when coupled to a BaF_2 scintillator (which has a fast component in the UV).The solid photocathode will become useful in practical devices if the ageing mechanism is understood and brought under control. The results of the research until July of 1991 have been presented in references 1 - 4, and are summarized in the enclosed Status Report of 7 August 1991. The researchers are David Anderson and Simon Kwan of the Particle Detector Group of FERMILAB, Vladimir Peskov of CERN (July and August of 1991) and Bruce Hoeneisen of Universidad San Francisco de Quito (summer of 1990 and August through October of 1991). In this progress report we present preliminary results obtained during July and August of 1991 on ageing, enhancement, time-of-flight resolution and new photocathodes.

2.- Work to date

a) We are preparing a test set up to measure the time resolution for time-of-flight applications. Two detectors have been built, and the NIM electronics and NaF crystals have been ordered. We expect to achieve a resolution of the order of 100 ps or better. The potential advantages over phototubes are compactness, relative insensitivity to a magnetic field, granularity and perhaps price.

b) During August we have made 5 photocathode evaporations for enhancement and ageing studies. 1.- Two microns CsI-TMAE on aluminum (6/8/91). 2.- 0.1 microns CsI-TMAE on aluminum (9/8/91). 3.- Two microns CsI-TMAE on copper (10/8/91). 4.- 0.5 microns CsI on aluminum with no TMAE adsorption (12/8/91). 5.- 15 nm CsI on aluminum with no TMAE adsorption (19/8/91). Next evaporation is due on 26/8/91.

c) Other photocathodes besides CsI have been tested: metals with low work function and some metaloorganic compounds.

3.- Preliminary results on ageing

a) Quantum efficiency. The initial quantum efficiency (measured by pulse counting and calibrating against the known quantum efficiency of TMAE gas as explained in references 1 and 2) was 14% at 190 nm for the photocathode evaporated on 6/8/91, and 16% at 190 nm for the photocathode evaporated on 9/8/91.

b) Enhancement of quantum efficiency. There are several ways to enhance the quantum efficiency of the photocathode. The group at CERN[5] observed a remarkable enhancement of the quantum efficiency from the initial value of order 15% to approximately 30% at 190 nm by flushing methane for several days. We have repeated this measurement and observed an enhancement due to methane flow at room temperature for 12 hours by a factor 1.66 over the initial efficiency of 16% at 190 nm.

In reference 3 it was found that an enhancement by a factor 1.7 over the initial quantum efficiency of 21% at 190 nm is achieved by initially operating the device in the diode mode at a low current density. We plan to study this effect in more detail in the near future.

Another way to enhance the quantum efficiency is to condense TMP or TMS on the photocathode surface[6]. We tryed to condense TMP on the CsI-TMAE photocathode, but did not see any noticeable increase of the quantum efficiency.

In the present work we observe enhancement of the efficiency of a freshly evaporated photocathode, or of a previously "aged" photocathode by increasing the temperature of the photocathode or by reducing the intensity of the UV light. This enhancement has been observed in vacuum, in methane and in helium. The enhancement seems to occur faster in vacuum. As an example, for spot #2 of the photocathode evaporated on 12/8/91 operated in the diode mode with the Hg UV source, we began at a current of 15.9 nA, which degraded at room temperature to 1.2 nA, and then recuperated to 6.8 nA by heating in vacuum to 97°C (the spot defined by the UV filter has a diameter of 12 mm). As another example, spot #1 of the photocathode evaporated on 12/8/91 was "aged" from 111 nA to 6.44 nA, and then recuperated back to 46 nA by heating to 97°C in vacuum. The enhancement obtained by heating the photocathode is not lost when the photocathode is brought back to room temperature or when the chamber is pumped to a vacuum of 10^{-5} Torr.

An "aged" photocathode recuperates slightly its efficiency by flushing TMAE gas. For example the photocathode evaporated on 6/8/91 had an initial efficiency of 14% at 190 nm, degraded to 1% by the ageing studies, and then recuperated to 1.8% by exposing to vapor pressure of TMAE and then pumping down to approximately 1 mTorr.

c) Description of "ageing". At room temperature the quantum efficiency of the photocathode reduces by a factor of e for a total accumulated charge of the order of 5 uC/mm^2, which corresponds to one elementary charge per 3 $Å^2$ of photocathode area. This

total accumulated charge has been observed at room temperature for photocathodes ranging in thickness form 15 nm to 2.3 μm, from a vacuum of 10^{-5} Torr to atmospheric pressure of methane, at gains from 1 to $1.4*10^6$, with light intensities that have been varied by a factor 21, and at high gain in methane, ethane and hexane. This "ageing" is partly or wholly reversible by heating the photocathode in vacuum, in methane or in helium; by flowing methane; or by reducing or turning off the UV source as explained in the previous section. When the voltage applied to the anode is reduced to zero the "ageing" or the enhancement continues at the same rate as with the voltage set to a low value corresponding to a gain of 1. When the applied voltage is reduced to zero the cathode current reverses sign indicating charging of the photocathode. For example, for the 2 um photocathode, changing the anode voltage from 48 V to 4 V changed the cathode current from +22.9 nA to -8.1 nA. The reverse current is much smaller for the thinner photocathodes. Of the order of 5 V are required to reduce the current to zero. Some enhancement is observed when a negative voltage is applied to the anode. "Ageing" is qualitatively the same for CsI photocathodes with or without adsorption of TMAE.

As a final example, the photocathode of 15 nm thickness was aged in a vacuum of 10^{-5} Torr at 22°C from 8.6 nA to 3.8 nA with a time constant of 70 minutes. This photocathode was then heated to 80°C. The current increased to 7.5 nA and then decreased with a time constant of 1528 minutes.

4.- Search for new photocathodes

CsI and CuI are not the only photocathodes that can be used. For example, it was discovered earlier[7] that metal surfaces covered by an adsorbed layer of TMAE increase their quantum efficiency, and that this efficiency is higher for the metals with the smalest work functions[5, 6].Other alternatives could be metaloorganic compounds which due to their molecular structure can combine a low ionization potential with resistance to air. In addition, according to a preliminary study[4], some of these compounds have better ageing properties than CsI. These studies have been continued at FERMILAB. Preliminary results obtained during July and August are as follows:

a) Metals with low work function. The metals with low work function (about 3 eV) Cd, Ho and Tb with adsorbed TMAE were tested. Typical quantum efficiencies obtained are 1 to 3% at a wavelength of 190 nm. The meassured cut-off is around 220 nm. We plan to continue work in this direction. We do not expect any ageing problems with these photocathodes.

b) Metaloorganic compounds. A few new metaloorganic compounds were tested: differrocenophanemercury, bisbencentrilchromine and 1-carboulmethane-pirromidinton 2.

The highest quantum efficiency achieved was 3% at 190 nm and corresponds to differocenophanemercury. The meassured cut-off is 230-240 nm. We plan ageing studies of these compounds.

5.- Comments on the physics

a) **Cross section of TMAE.** At 20°C the vapor pressure of TMAE is 0.325 Torr and the photon mean free path at 200 nm is 30 mm. Then the TMAE molecule absorption cross section is

$$\sigma = \frac{V}{LN} = \frac{kT}{LP} = 0.315\ A^2$$

If a TMAE molecule covers about 10 A^2 of photocathode surface, then about 3% of the UV photons are absorbed by the monolayer of TMAE and the remaining 97% by the CsI. This estimate is in agreement with the enhancement of the quantum efficiency of metals by adsorbed TMAE.

b) **Charging of the photocathode.** The photocathode "ages" at an accumulated total charge of order 5 uC/mm^2. If the photocathode were perfectly insulating the voltage across a 1 um photocathode with this charge density would be about $6 \cdot 10^5$ V/e_r. Therefore less than one elementary charge in 10^5 stays in or on the photocathode. What is the conduction mechanism? Perhaps the high electric field provides an ohmic contact between the CsI and the metal by tuneling.

b) **Ageing mechanisms.** As we have noted above, at room temperature we frequently observe that the quantum efficiency decreases by a factor e at an accumulated total charge of order 5 uC/mm^2, which is equivalent to one elementary charge per 3 Å^2. This observation suggests the following tentative model of "ageing":

The quantum efficiency drops due to a monolayer of "molecules" covering the photocathode by adsorption. These "molecules" are produced or set free by the UV photons (and the avalanche). These molecules may be water, iodine or hydrocarbon radicals.

Let us recall that adsorption is a state of equilibrium between molecules attached with energy -E to sites on the surface, and the same molecules in the "gas" phase. The probability that a surface site is occupied is given by

$$p = \frac{1}{1+\exp\left[-\frac{E+\mu}{kT}\right]}$$

where

$$\mu = \ln\left[v_Q \frac{N}{V}\right]$$

is the chemical potential of the molecules, and N/V is their number density. μ is negative since for an ideal gas V/N is much larger than the quantum volume v_Q.

μ becomes more negative at low concentration N/V, i.e. with no UV light and with strong methane flow or high vacuum. Then the probability p is low and the quantum efficiency is high. Conversely, μ approaches zero at high concentration N/V, i.e. with intense UV light and no flow of methane. In this case the probability p approaches 1 at low temperature, the surface becomes covered and the quantum efficiency is very small.

In general this is what is observed. The time constant to reach equilibrium is of the order of 100 minutes. This model explains why enhancement of the quantum efficiency is achieved by the tree methods: methane flow, low initial current density (i.e. low UV intensity), and heating. The model is also compatible with the observation that ageing is relatively independent of photocathode thickness. We have however observed ageing with low light intensities even with methane flow.

6.- What next?

We will do the following studies during the next couple of months. Continue enhancement and ageing studies. What "molecules" cover the photocathode? Measure the time-of-flight resolution. Study the CuI photocathode which is stable in air and should have better "ageing" characteristics (5% efficiency at 200 nm but cutoff at 350 nm, dissolves in alcohol, and is a conductor). Study iodides of Cd, Ho and Tb. Determine the optimum anode-to-cathode distance that gives maximum gain.

7.- Conclusions

During this month we have advanced our understanding of "ageing": **it is not ageing at all** since it is reversible! The simple model described in section 4 generally explains the observations. Will practical devices for RICH, time-of-flight and calorimetry emerge? It will depend on the outcome of the ageing and enhancement studies of CsI and CuI and other metal iodides. We hope to be able to answer this question in the near future.

Acknowledgement:

We thank the technical support of Sharon Austin, Eileen Hahn and Jerry Zimmerman.

References:

(1) "Report #12 on the Bottom Collider Detector: Fast Imaging Ultraviolet Detector", B. Hoeneisen, D.F. Anderson, S. Kwan and M. Adams, BCD, unpublished.

(2)"A CsI-TMAE photocathode with low-pressure readout for RICH", B. Hoeneisen, D.F. Anderson and S. Kwan, NIM A302 (1991) 447-454.

(3)"A study of the CsI-TMAE photocathode", S. Kwan and D.F. Anderson, submitted to NIM.

(4)"New photocathodes for fast gaseous detectors", Preprint CERN PPE/90-185.

(5)J. Sequinot et al, NIM A297 (1990) 133.

(6)V. Peskov et al, NIM A269 (1988) 149.

(7)D.F. Anderson, Phys. Lett. 118 (1982) 230.

B. H. & V. P.
21 August 1991

TM-1753
September 1991

Technical Memo on New Results on CsI Photocathodes: Enhancement and Aging

D.F. Anderson, B. Hoeneisen[1], S. Kwan, and V. Peskov[2]
Particle Detector Group
Fermi National Accelerator Laboratory
Batavia IL 60510 U.S.A.

Abstract

It appears that there are 4 processes involved in the enhancement and aging of a CsI or CsI-TMAE photocathode: water absorption, charging up of the photocathode, a self annealing aging, and a permanent aging. The evidence for these processes are presented.

---

[1]Universidad San Francisco de Quito, P.O. Box 17-1200841, Quito, Ecuador
[2]CERN/World Lab, Geneva Switzerland

Introduction

The use of pure CsI or CsI-TMAE as a photosensitive element in wire and parallel plate chambers has been recently demonstrated [1-3]. Detectors with this solid photocathode have a better time resolution than the conventional detectors with photosensitive vapors. In fact it is a new type of detector, which some authors call gaseous photomultipliers [4]. However large scale applications of this device have been restricted due to the aging of the CsI photocathode [3-6]. Some authors [5,7,8] have observed enhancement of the quantum efficiency of the CsI photocathode under some conditions which in principle could compete with aging.

In this Technical Memo we report our latest results on the aging and enhancement properties of the CsI and CsI-TMAE photocathodes. It is intended to be an informal (but referential) communication to those working in the field.

Experimental set-up

The parallel plate avalanche chamber used for this study is shown in fig. 1. It is similar to the one described in references 3 and 5, except that it contains a cathode that can be cooled or heated between -20 and +100 °C. The chamber was evacuated to a pressure of 10^{-4} when operated in the diode mode. Measurements with gain were also made at pressures of 10 Torr to 1 atm. The quantum efficiency of the photocathode is measured relative to the known efficiency of TMAE gas as described in reference 3. The ultraviolet light source used is a Hg lamp with its intensity monitored by a photodiode. For most of the measurements the UV light passed through a filter at $\lambda \approx$ 185 nm or through a monochrometer. The area of the illuminated spot on the photocathode for all measurements was 113 mm^2. Several photocathodes were tested: 0.5 and 0.015 μm pure CsI, and 2 and 0.1 μm of CsI with an adsorbed TMAE layer as described in reference 3.

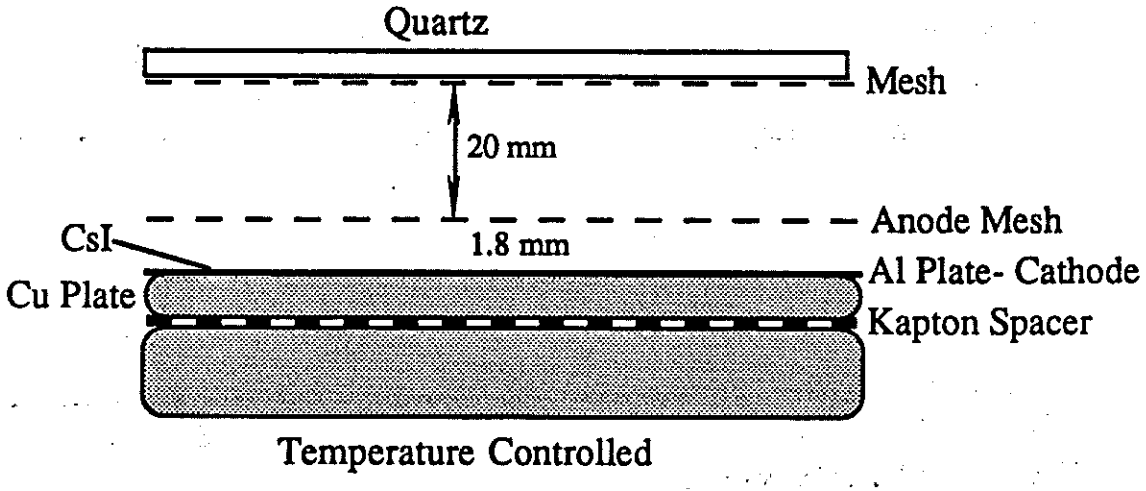

Figure 1. Parallel plate avalanche chamber with solid photocathode.

Measurements

We observed the current (which is proportional to the quantum efficiency, QE, of the photocathode) in the chamber for pressures ranging from 10^{-4} to 1 atm and for gas gains that varied from 1 to 10^6. A typical measurement for a 0.1 μm thick CsI-TMAE photocathode with 20.4 Torr of methane and a gas gain of 262 is shown in Fig. 2. From time 0 to t_1 the photocathode is illuminated with intense UV light. The current (and QE) decreased as shown. At time t_1 the light was blocked and the quantum efficiency restores in time as shown by momentarily unblocking the UV light at times t_2 - t_5. These results are typical at room temperature operation at all pressures and gains studied.

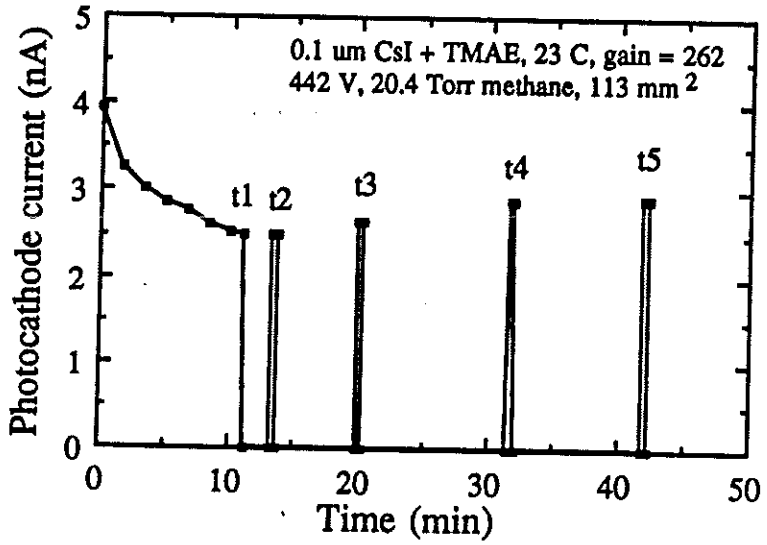

Figure 2. Current of a CsI-TMAE photocathode as a function of time for a typical measurement. The gas gain is 262 and the pressure is 20.4 Torr of methane. The UV light is interrupted at time t1, and reestablished for a moment at times t_2-t_5.

Fig. 3 shows the response of a pure CsI photocathode 0.015 μm thick in vacuum with a collection voltage of 11 V. We observe the same degradation of the QE as seen in the early part of fig. 2 at room temperature. At time t_1 the photocathode heater is turned on. The efficiency initially decreases by a few percent, then raises significantly, and finally slowly decreases again when the temperature stabilizes. The rate of aging at 80°C is much less than for room temperature. A similar enhancement by a factor ≈ 1.7 is observed when heating a freshly evaporated photocathode to 97 °C. This enhancement is not lost by a return to room temperature or by pumping to 10^{-3} Torr.

It is interesting to note that when a similar measurement to the one in fig. 3 was made with pure He as the counter gas at a gain >1, at the point that the heater was turned on there was a sudden, transient increase in the current. This is most likely due to the outgassing of something from the photocathode. The gas, having a lower ionization potential than the

first excited state of He, causes an increase in current by the Penning effect. This effect is seen for both CsI and CsI+TMAE photocathodes.

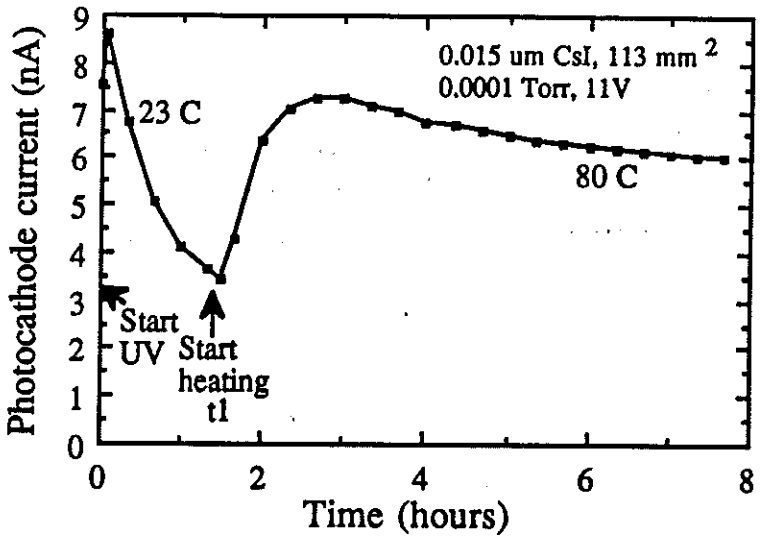

Figure 3. Current as a function of time for a CsI photocathode. At time t_1 the photocathode is heated to 80 °C.

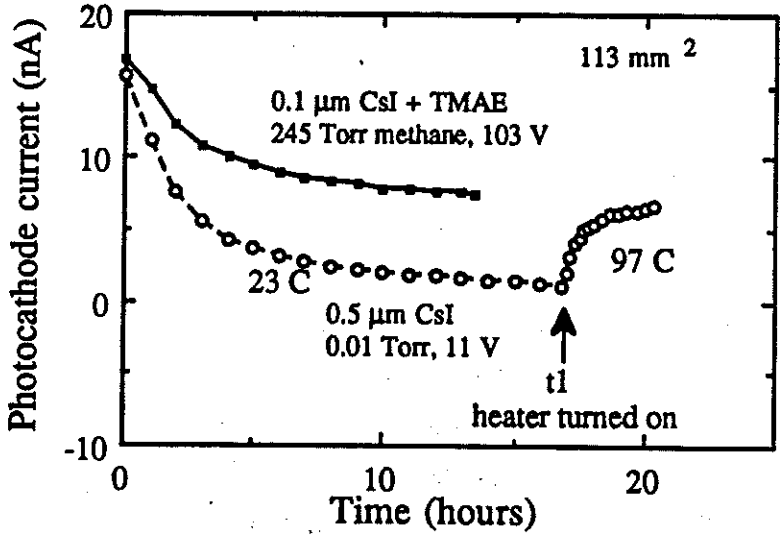

Figure 4. Currents as a function of time for a 0.1 µm thick CsI+TMAE and a 0.5 µm thick CsI photocathode.

In fig. 4 we compare the aging properties of a particular CsI photocathode to those of a particular CsI-TMAE photocathode, both at room temperature. Initially the drop in current is similar for both photocathodes, but with the current of the CsI-TMAE photocathode showing a smaller degradation The enhancement of the QE of the CsI photocathode, when it is heated, is also shown.

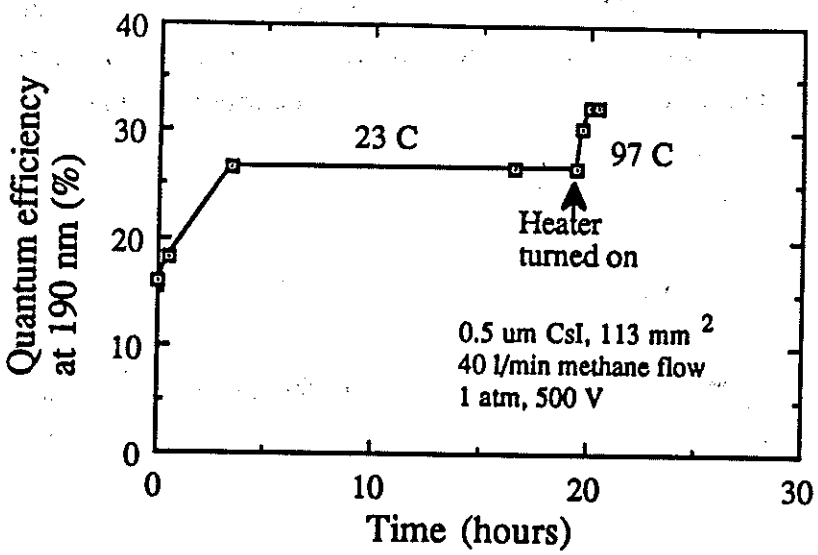

Figure 5. QE as a function of time of a freshly deposited , 0.5 μm thick CsI photocathode with a 40 l/min flow of methane. At 20 hours the photocathode is heated to 97 °C.

There is one other measurements that also relates to the the phenomenon of enhancement. Fig.5 which shows the QE at λ=190 nm of a freshly evaporated 0.5 μm CsI photocathode operated at 1 atm with a 40 l/min flow for pure methane, initially at 23 °C. The QE increases with time a and plateau is reached at about 27%. This is a similar result to that seen by others [8] but it is achieve on a shorter time scale. At t=20 hours the cathode was heated to 97 °C and there is an almost instantaneous jump in QE to about 34%. This result will be interpreted in the next section.

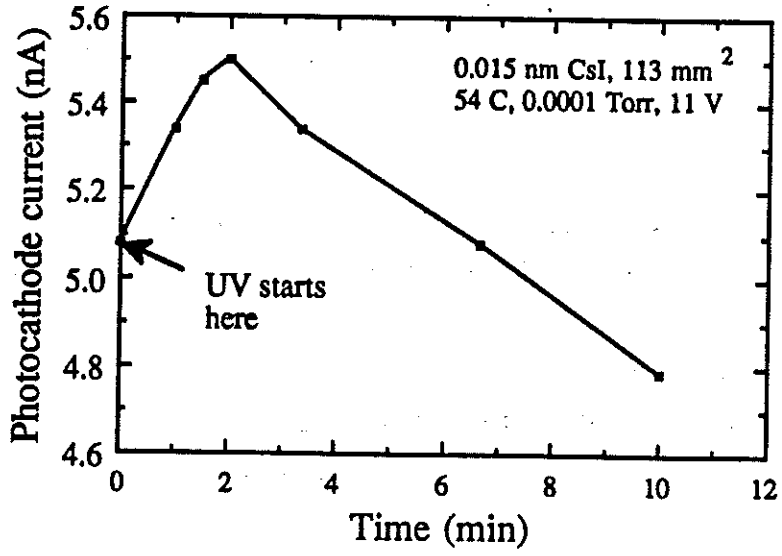

Figure 6. Current as a function of time for a CsI photocathode showing the initial enhancement seen in almost all measurements.

In fig. 6 we present the initial enhancement of the quantum efficiency when the UV light is unblocked and when the chamber is operated at a relatively high vacuum (10^{-4} Torr) and a gain of 1. There is an initial increase in current (QE) before the degradation. This phenomenon is same as the one reported in an earlier work [5]. See fig. 3 for another example of this effect.

Working Hypotheses

Many measurements have been made. Not all of the results can be presented in this Technical Memo. We have developed a working hypotheses which seems to explain our results to date and will be used to direct future research. Our hypotheses is that there are four major phenomena involved:

1. Water absorbed by the photocathode lowers the QE. This water can be removed by vacuum, heating, or a flow of dry gas and explains the enhancement seen in fig. 5. These results explain the enhancement that Séguinot et al.[8] see with the flowing of clean methane.

2. A charging up of the photocathode, increasing the QE. This is seen in figs. 3 and 6 . The enhancement seen by Anderson and Kwan [5] now appears to be due to charging up of the photocathode.

3. An unidentified reversible process of aging and recovery of the surface of the photocathode. It is induced by UV photons and positive ions of the avalanche. At a gain of 1 the charge saturates this process at $\approx 5\ \mu C/mm^2$, equivalent to one elementary charge per $3 Å^2$. The recovery rate increases with temperature, yielding a higher equilibrium QE with higher temperature. As one would expect, the aging process is related to the current intensity, with a higher equilibrium QE for lower currents. See figs. 2 and 3.

4. An unidentified irreversible aging process that determines the long term rate of decrease of efficiency after the reversible phenomena have reach equilibrium.

Acknowledgement:

The authors would like to thank SSClab, Professor Zichichi, and the World Lab for support of this work. We would also like to thank the technical support of Sharon Austin, Eileen Hahn and Jerry Zimmerman.